Shear transfer mechanism in reinforced engineered cementitious composite (ECC) beams: Quantification of Vs and Vc

Gu, D.; Pan, Jinlong; Mustafa, S.; Huang, Y.; Lukovic, M.

DOI
10.1016/j.engstruct.2022.114282

Publication date
2022

Document Version
Final published version

Published in
Engineering Structures

Citation (APA)
Gu, D., Pan, J., Mustafa, S., Huang, Y., & Lukovic, M. (2022). Shear transfer mechanism in reinforced engineered cementitious composite (ECC) beams: Quantification of Vs and Vc. *Engineering Structures*, *261*, Article 114282. https://doi.org/10.1016/j.engstruct.2022.114282

Shear transfer mechanism in reinforced engineered cementitious composite (ECC) beams: Quantification of Vs and Vc

Gu, D.; Pan, Jinlong; Mustafa, S.; Huang, Y.; Lukovic, M.

DOI
10.1016/j.engstruct.2022.114282

Publication date
2022

Document Version
Final published version

Published in
Engineering Structures

Citation (APA)
Gu, D., Pan, J., Mustafa, S., Huang, Y., & Lukovic, M. (2022). Shear transfer mechanism in reinforced engineered cementitious composite (ECC) beams: Quantification of Vs and Vc. *Engineering Structures*, *261*, [114282]. https://doi.org/10.1016/j.engstruct.2022.114282

Shear transfer mechanism in reinforced engineered cementitious composite (ECC) beams: Quantification of Vs and Vc

Gu, D.; Pan, Jinlong; Mustafa, S.; Huang, Y.; Lukovic, M.

DOI
10.1016/j.engstruct.2022.114282

Publication date
2022

Document Version
Final published version

Published in
Engineering Structures

Citation (APA)
Gu, D., Pan, J., Mustafa, S., Huang, Y., & Lukovic, M. (2022). Shear transfer mechanism in reinforced engineered cementitious composite (ECC) beams: Quantification of Vs and Vc. *Engineering Structures*, *261*, [114282]. https://doi.org/10.1016/j.engstruct.2022.114282

Engineering Structures 261 (2022) 114282

Contents lists available at ScienceDirect

Engineering Structures

journal homepage: www.elsevier.com/locate/engstruct

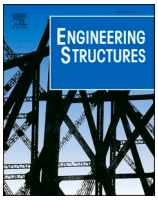

Shear transfer mechanism in reinforced engineered cementitious composite (ECC) beams: Quantification of V_s and V_c

Dawei Gu [a,b], Jinlong Pan [a,*], Shozab Mustafa [b], Yitao Huang [b], Mladena Luković [b]

[a] School of Civil Engineering, Southeast University, Nanjing, China
[b] Faculty of Civil Engineering and Geosciences, Delft University of Technology, Delft, Netherlands

ARTICLE INFO

Keywords:
Engineered Cementitious Composite (ECC)
Strain Hardening Cementitious Composite (SHCC)
Shear
Stirrup

ABSTRACT

To enhance the structural and seismic resistance, as well as durability of concrete structures, an ultra ductile fiber reinforced cementitious composites called Engineered Cementitious Composite (ECC), also known as Strain Hardening Cementitious Composite (SHCC), was developed. ECC has a similar compressive and tensile strength to conventional concrete, but it exhibits a pseudo-strain-hardening behaviour under uniaxial tension with excellent crack control ability. The ultimate tensile strain of ECC can reach 3–12%, which is 300–1200 times higher than that of concrete. It is reported that ECC can also exhibit at least twice as high shear carrying capacity compared to traditional concrete, signifying a potential to use ECC material in shear-resistance elements. However, the shear resisting mechanism of reinforced ECC (R/ECC) members is still not clear. In most existing codes and models, the shear strength of reinforced structural members (V_u) is divided into two parts, i.e., shear resistance coming from the matrix (V_c) and from the transverse reinforcement (V_s). To quantify accurately V_c and V_s and also their development throughout the loading, a well-designed testing method consisting of continuous strain quantification along the stirrups, was used in this research. Six steel reinforced beams incorporating different matrix (ECC, concrete and mortar) were tested under four-point bending. The test results indicated that V_c changed continuously with the propagation of shear crack, whereas the stirrups that crossed the critical shear crack, did not always yield at the ultimate shear resistance.

1. Introduction

Engineering Cementitious Composite (ECC) is a fiber reinforced material tailored with a special micromechanical design to enable steady state cracking with small crack widths [1,2]. As a result, ECC exhibits pseudo strain hardening behaviour with multiple cracking under uniaxial tension. Compared to traditional concrete, ECC has similar compressive and tensile strength, but has hundreds times higher tensile strain capacity (ranging from 3 to 12%) [2]. Due to outstanding deformation capacity, utilizing ECC in structural members can prevent catastrophic collapse, for example during earthquakes, enabling lives savings and reducing repair costs [3,4]. Additionally, the maximum crack width in ECC can be limited to less than 0.1 *mm* until its ultimate strain, revealing a potential to enhance the durability of reinforced concrete structures under severe environmental conditions [5–8]. ECC has already been widely applied for various field constructions including buildings, transportation, water and other infrastructures [9–16]. However, there is still lack of comprehensive understanding about structural behaviour and, more specifically shear transfer mechanism of reinforced ECC (R/ECC) members and reliable models to predict this behaviour.

For shear behavior of structural members, the assumption that '*plane remains plane*' for cross-sectional analysis does not hold as in the case of flexure. For conventional reinforced concrete (RC) members, different shear failure modes including shear-tension, shear-compression and diagonal compression would happen depending on its member dimensions and loading conditions, reinforcement distribution, material strength, aggregate size, etc. Over twenty parameters influence its ultimate shear strength. In order to provide simplified design rules, various analytical models for predicting shear strength of RC members have been established over the past century, including the early truss model proposed by Ritter [17] and Mörsch [18,19], modified compression field theory (MCFT) [20–22], rotating-angle softened-truss model (RA-STM) [23,24], fixed-angle softened-truss model (FA-STM) [25,26], strut and tie model [27,28], among others. Until now, there is no unified theory,

* Corresponding author.
E-mail addresses: dwgu@seu.edu.cn (D. Gu), cejlpan@seu.edu.cn (J. Pan), s.mustafa-2@tudelft.nl (S. Mustafa), y.huang-6@tudelft.nl (Y. Huang), m.lukovic@tudelft.nl (M. Luković).

https://doi.org/10.1016/j.engstruct.2022.114282
Received 6 December 2021; Received in revised form 9 April 2022; Accepted 13 April 2022
Available online 26 April 2022

Nomenclature

V_u	total shear carrying capacity
V_c	shear force carrying by matrix
V_s	shear force carried by transverse reinforcement
V_{cd}	dowel force of longitudinal tensile reinforcement
V_a	shear force carried by intact matrix in shear compression zone
C	resultant compressive force of intact matrix in shear compression zone
T	resultant tensile force of longitudinal tensile reinforcement
S	aggregate interlock force along diagonal shear crack
σ_{fiber}	fiber bridging stress along diagonal shear crack
ϕ	inclination angle of diagonal shear crack
n	total number of transverse rebars
V_{si}	force of ith stirrup leg
$f_c^{'}$	compressive strength of matrix
f_{ty}	nominal tensile yield strength of ECC
f_{tu}	tensile strength of ECC
ε_{tu}	ultimate tensile strain
ρ_l	tensile reinforcement ratio
ρ_t	shear reinforcement ratio
a	shear span length
d	effective depth of beam section
v	average shear stress
V	shear force
b	beam width

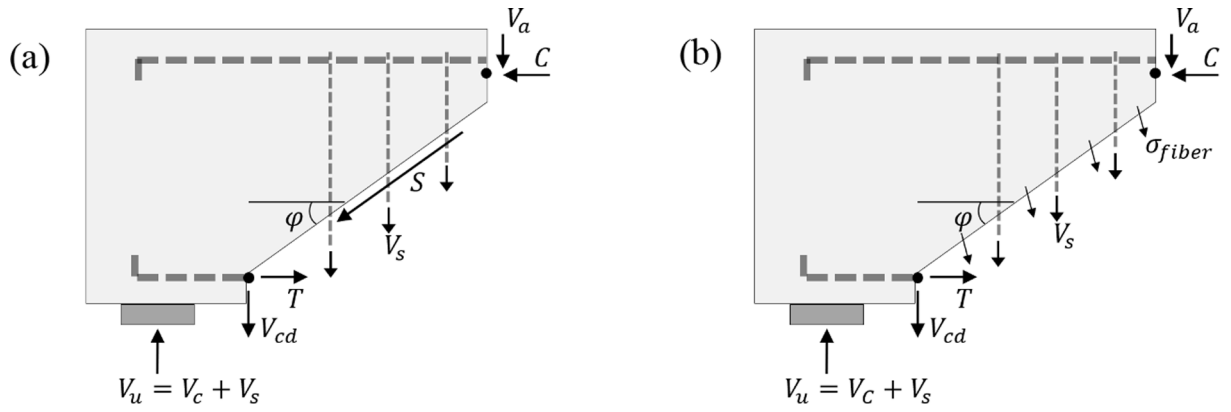

Fig. 1. Components of shear resistance for (a) RC beams; (b) R/ECC beams.

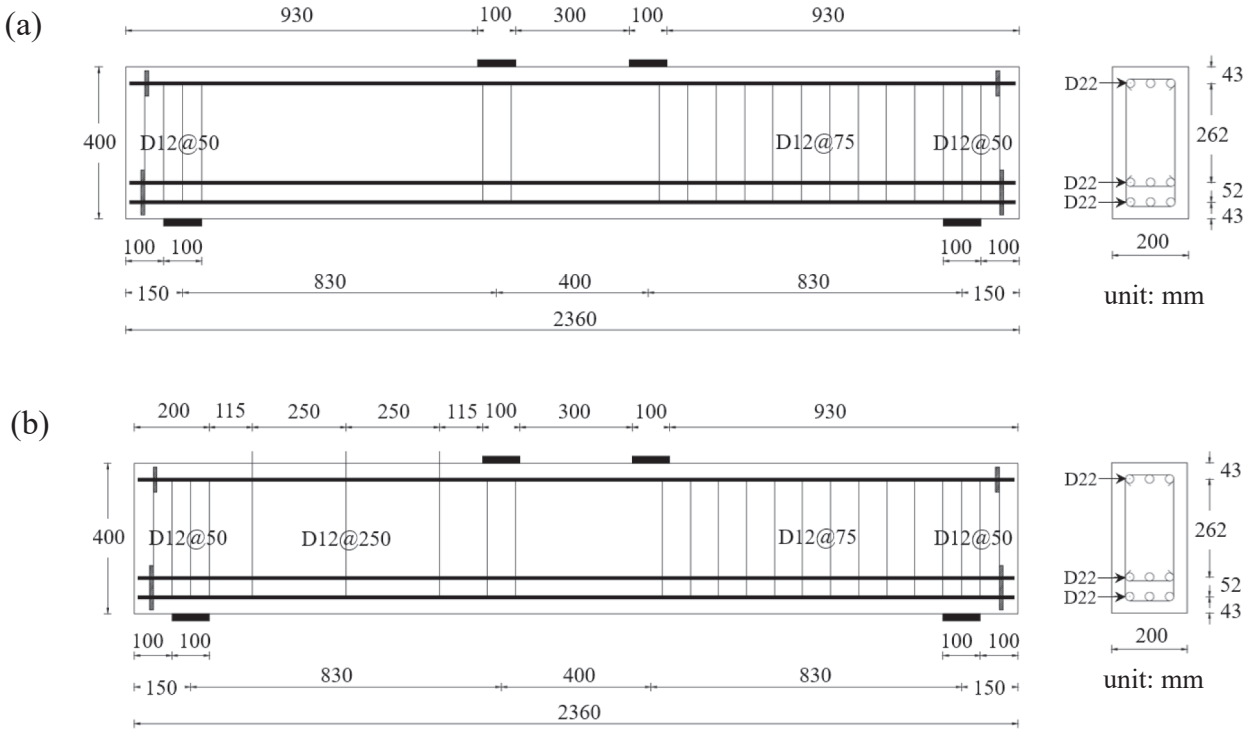

Fig. 2. Details of beam specimens: (a) C-N, E-N and M−N; (b) C-S, E-S and M−S.

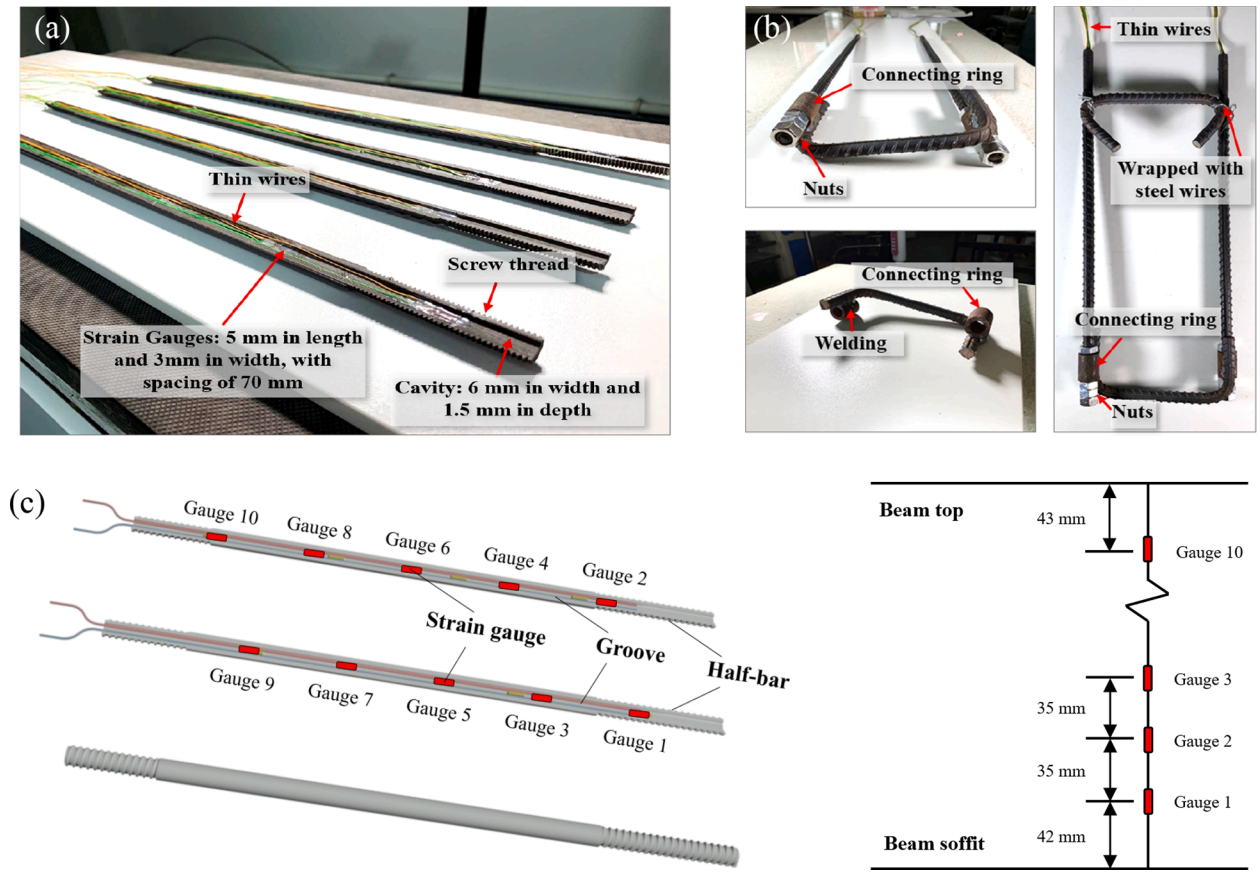

Fig. 3. Strain gauging system for stirrups: (a) cavity inside stirrup legs; (b) assembled stirrups; (c) layout of strain gauges.

code or specification for shear design of RC members that is worldwide accepted. Large discrepancy among various codes sometimes exists when estimating shear strength of RC members, signifying potential waste of resources or sometimes dangerous overestimation of structural safety [29].

Due to the characteristic strain hardening behavior and crack control ability, steel reinforced ECC exhibits different shear transfer mechanism compared to RC. When referring to the material itself, the shear strength and ultimate shear strain of ECC was reported to be over 2 and 22 times, respectively, that of plain concrete [30]. In an Iosipescu shear test, rotation of principal stress was observed due to fiber's bridging across shear cracks, which resulted in ECC's nominal shear strength exceeding its direct tensile strength by up to 50% [31]. When reinforced with steel, incorporating ECC can alter the brittle shear failure into ductile flexure failure [32–34]. Multiple cracking behavior can also be observed, with crack width being 3 to 5 times smaller than those in RC at similar load level [35]. For beams without stirrups, the shear strength and ultimate displacement of R/ECC can be 1.5 and 2 times that of RC [36]. When mixed with different quantity of PVA fiber, it was found that the shear carrying capacity of R/ECC beams almost linearly increased with fiber's volume fraction, revealing significant contribution from fibers in resisting shear force [37–39].

Until now, very limited theoretical or empirical models, codes or specifications have been established for the shear design of R/ECC members. For conventional concrete, the superposition methodology has been most widely adopted for shear design in various design regulations, in which the total shear carrying capacity (V_u) is divided into resistance from concrete (V_c) and stirrups (V_s), as shown in Fig. 1 [40–43]. The same idea is adopted by the ECC standard specification JSCE 08 [44], in which the fiber's contribution is also considered in calculating V_c. Based on regression analysis of test data, Hou et al. [33,34] proposed an empirical formulation for calculating V_c and V_s for R/ECC members. When stirrups are used, a negative effect was found between shear resistance from ECC (V_c) and transverse reinforcement (V_s) [34]. Kanakubo et al. [37–39] proposed an analytical model for estimating V_c and V_s in R/ECC based on truss-arch shear transferring mechanism, where V_c is composed of fiber bridging stress across shear cracks and shear resistance from ECC compression zone. Although these models have been acknowledged as effective for calculating the total shear strength of R/ECC beams under certain circumstances, no research has been reported to evaluate V_c and V_s separately to enable in-depth verification of models.

In this research, a continuously-distributed strain gauging system is adopted, which can help measure the strain along full length of stirrups and longitudinal rebars for evaluating the variation of V_c and V_s in R/ECC members during loading. It provides a new insight into the mechanical interaction between ECC and steel reinforcement when shear failure predominates. As a pilot work, a total of six reinforced beams incorporating three types of matrices (ECC, concrete and mortar) with or without stirrups are tested under four-point bending. The load–deflection behavior, crack propagation, strain development in rebar, and variation of shear strength components are studied in detail. Finally, the existing models for predicting shear transfer mechanism are evaluated and critically assessed.

2. Experimental program

2.1. Details of beam specimens

Two ECC beams with and without stirrups and two concrete counterpart beams were fabricated. To evaluate the shear resisting contribution from fibers in ECC and coarse aggregates in concrete, another two reference mortar beams were cast. All beams had the same geometry, with cross section of 200 mm in width, 400 mm in height and 2360 mm

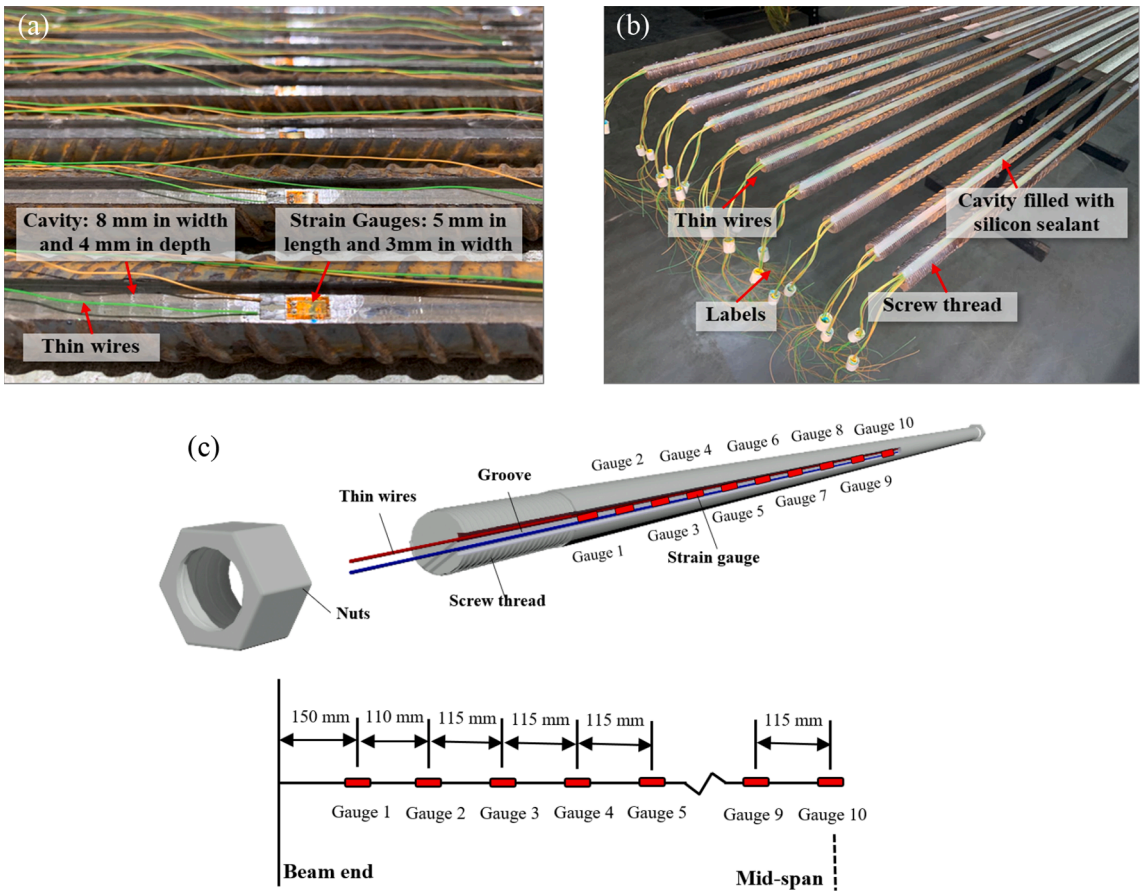

Fig. 4. Strain gauging system for longitudinal reinforcement: (a) cavity on rebars; (b) full view of rebars; (c) layout of strain gauges.

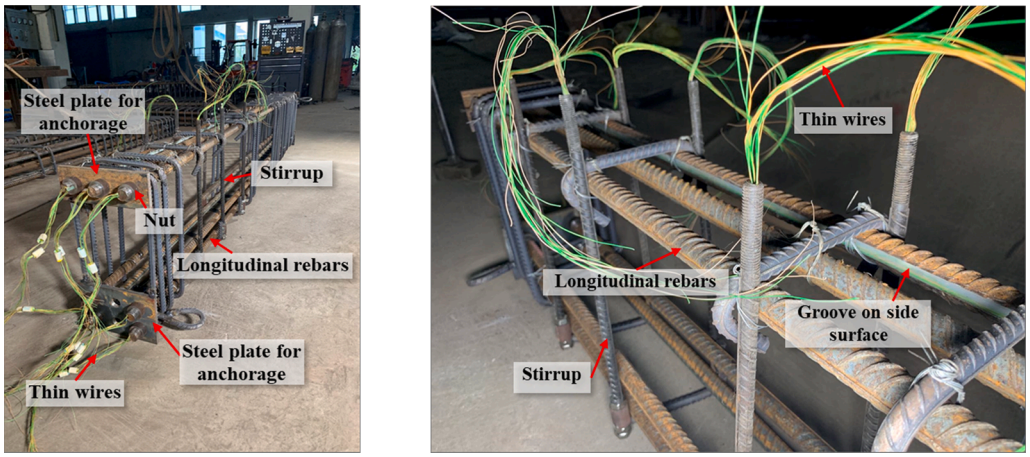

Fig. 5. Typical reinforcement cage.

in length. The shear span to effective depth ratio was 2.5, with a relatively high tensile reinforcement ratio of 3.2% to prevent undesired flexural failure during loading. To reduce the cost, half of the beam span was designed as monitoring zone to exhibit shear failure and equipped with the continuously-distributed strain gauging system. Detailed reinforcement configuration for all specimens is shown in Fig. 2. For the specimen notation, C-N, E-N and M−N represent the reinforced concrete, ECC and mortar beam without stirrups, respectively; C-S, E-S and M−S represent the same sequence of beams reinforced with stirrups, with a spacing of 250 mm and shear reinforcement ratio of 0.38%.

2.2. *Continuously-distributed strain gauging system for rebars*

For evaluating shear strength components, V_s can be calculated by summation of transverse forces in stirrups which intersect the critical shear crack. The transverse force for each stirrup leg should be determined by its strain at the shear crack location. However, it is hard to predict the shear crack path prior to experiments, therefore it is almost impossible to catch the stirrup strain exactly along the critical shear crack by installing only one strain sensor on surface of stirrup leg, no matter at mid-height or along assumed cracking path as depicted in most literatures [45–50]. Hence, the governing mechanisms that lead to shear

Table 1
Mixture proportions (kg/m^3).

	Concrete	ECC	Mortar
Cement (P.O 42.5)	584	426	426
Fly ash (grade II)	—	647	647
Cenosphere	—	162	162
Silica fume	31	43	43
Quartz powder	—	256	256
Sand 0–5 mm	596	—	—
Aggregate 5–10 mm	100	—	—
Aggregate 10–20 mm	964	—	—
Water	185	332	332
PVA fiber	—	26.8 (2.0%)	—
Superplasticizer	0.5	1.6	1.6
Hypromellose	—	0.5	0.5

failure can be misunderstood due to the lack of accuracy of the traditional strain detecting scheme. To obtain more accurate V_s, the use of distributed Fiber-Optic strain Sensors (FOS) is a promising way. By installing distributed FOS on surface of longitudinal and transverse reinforcement, Poldon et al. [51,52] identified and quantified a number of mechanisms for RC members with a new level of detail, including the strain variations along tensile and shear rebars, bending of longitudinal rebars from stirrup hook anchorage. Wu and Hu [53–55] also proposed a new methodology for measuring the strains along the full length of stirrups without disturbing the bond between concrete and steel. That is, cutting the stirrup leg into two halves, and installing strain gauges continuously inside a small cavity at the center of the bar. With such a full record of strain, V_c and V_s can be assessed accurately throughout the loading process. To evaluate two shear strength components V_c and V_s

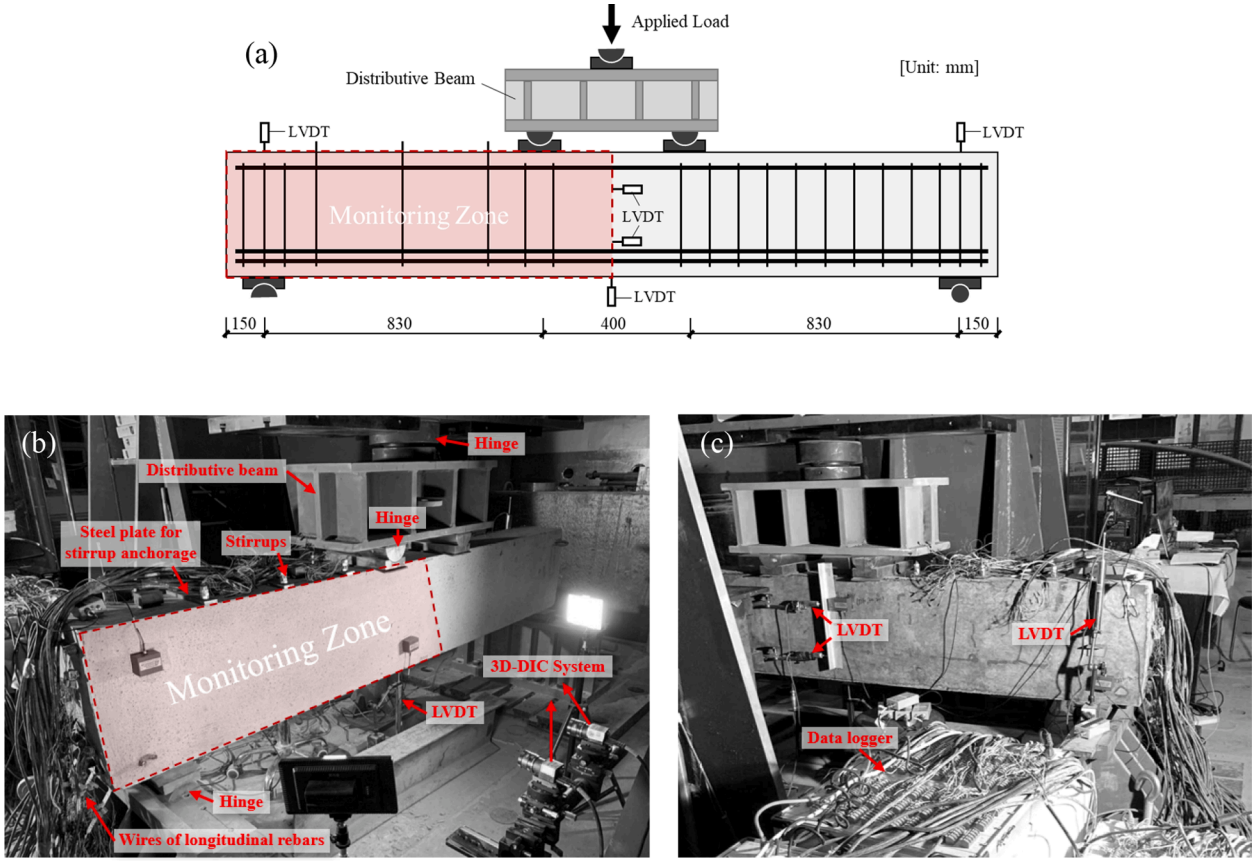

Fig. 6. Test setup: (a) schematic illustration; (b) front view indicating DIC monitored zone; (c) back view indicating LVDTs and monitoring devices from the opposite side.

Table 2
Summary of beam specimens and test results.

Specimen ID		Matrix type	Testing age (days) (days)	f_c' (MPa)	f_{ty} (MPa)	f_{tu} (MPa)	ε_{tu} (%)	ρ_l (%)	ρ_t (%)	a/d	V_u (kN)
C-N	Without Stirrup	Concrete	66	56.6	—		—	3.2	0.00	2.5	172.7
E-N		ECC	85	56.4	6.4	8.0	3.5	3.2	0.00		289.5
M−N		Mortar	70	55.4	—		—	3.2	0.00		144.4
C-S	With Stirrup	Concrete	86	53.0	—		—	3.2	0.38	2.5	359.8
E-S		ECC	100	54.7	6.1	7.5	3.8	3.2	0.38		421.4
M−S		Mortar	86	60.2	—		—	3.2	0.38		236.6

Note: f_c' = compressive strength; f_{ty} = nominal tensile yield strength of ECC; f_{tu} = tensile strength of ECC; ε_{tu} = ultimate tensile strain; ρ_l = tensile reinforcement ratio; ρ_t = shear reinforcement ratio; a/d = shear span to effective depth ratio; V_u = shear carrying capacity.

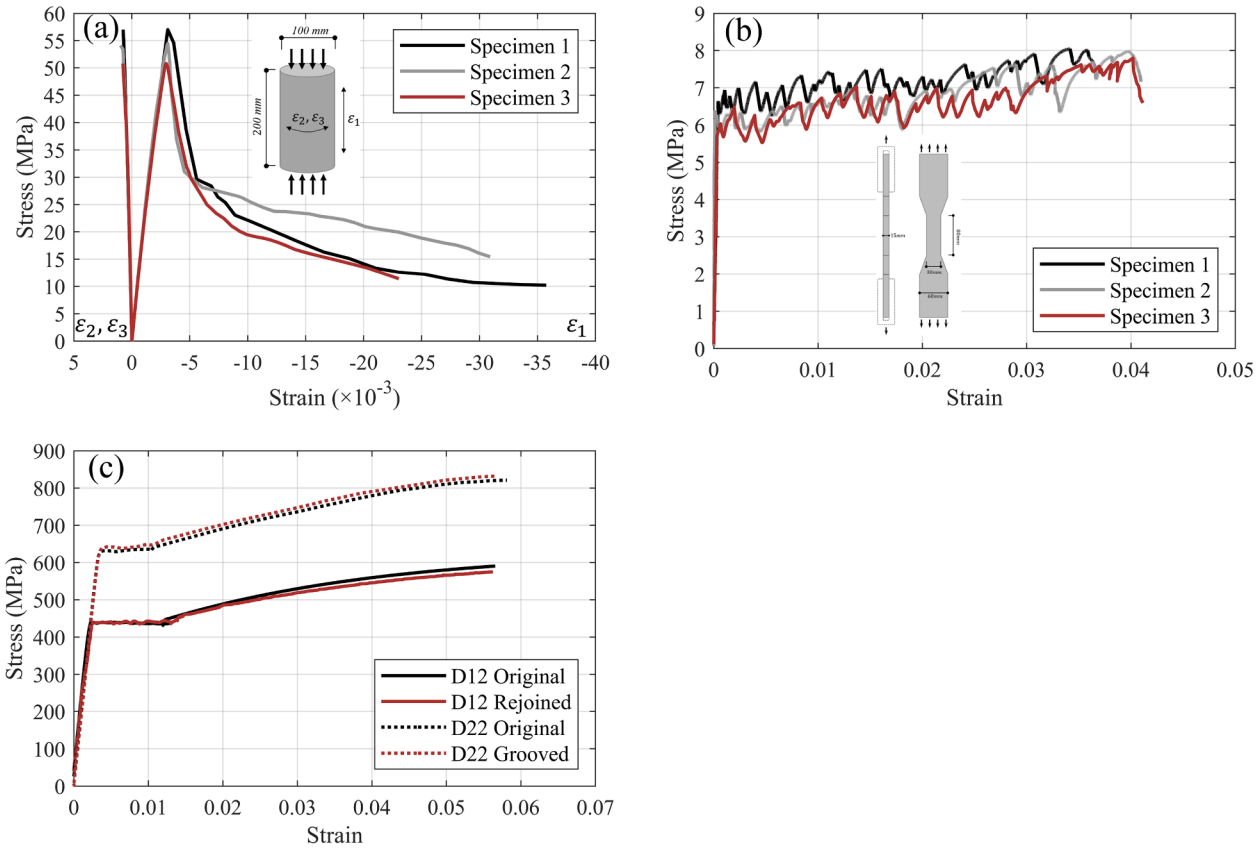

Fig. 7. Stress–strain relationship for: (a) ECC under uniaxial compression; (b) ECC under uniaxial tension; (c) steel rebars under uniaxial tension.

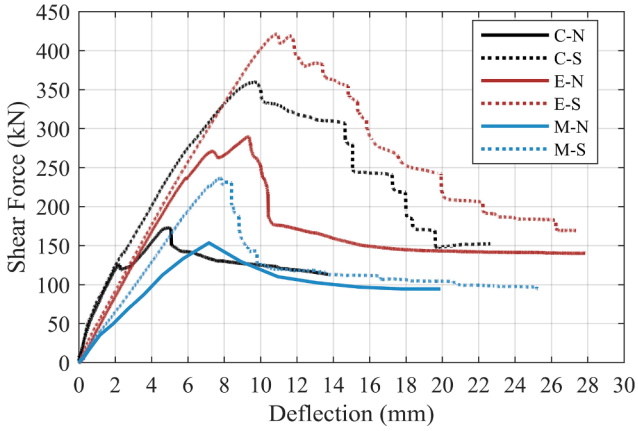

Fig. 8. Shear force–deflection curve for all beam specimens.

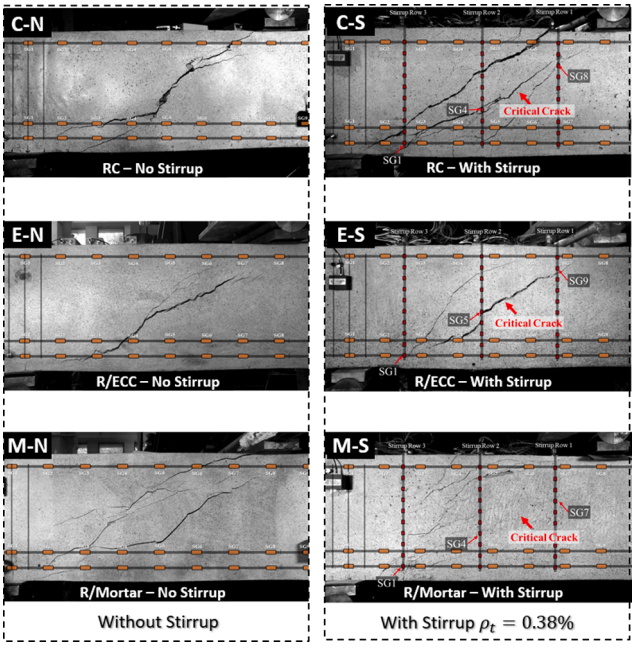

Fig. 9. Crack pattern at ultimate failure for beam specimens.

for R/ECC beams, such strain measuring system is adopted in this work.

The stirrup legs with diameter of 12 mm were cut into two halves longitudinally, and a cavity of 6 mm in width and 1.5 mm in depth was made at the center of each half-bar, as shown in Fig. 3(a). A set of strain gauges with length of 5 mm and spacing of 70 mm were attached in the cavity. The position of strain gauges for each stirrup leg is illustrated in Fig. 3(c). Since the heat of welding can cause the damage of strain gauges, two half-bars were connected by high strength epoxy resin instead of being welded together. The cavity was then filled with silicon sealant to prevent that water penetrates during casting of concrete or ECC. After that, two stirrup legs were assembled by a U-shaped steel bar with two connecting rings and a set of nuts, as shown in Fig. 3(b). With such strain gauging scheme, the shear strength components can be determined by following equation:

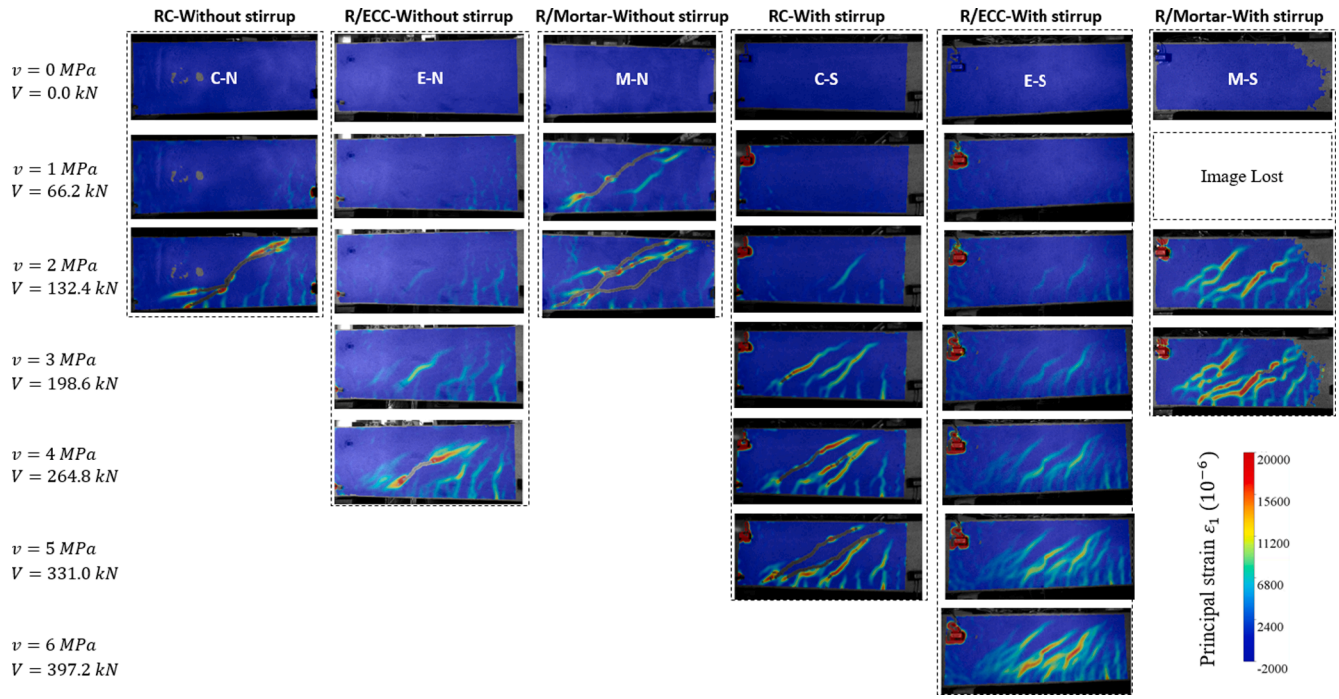

Fig. 10. Principal strain distribution in RC, R/ECC and R/mortar beams at different average shear stress.

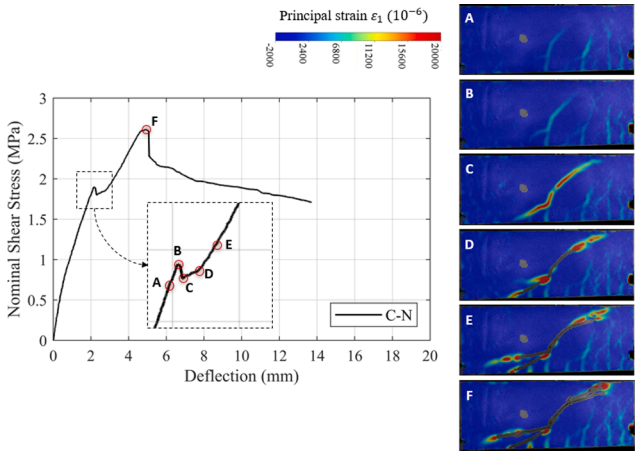

Fig 11. Cracking patterns at selected load levels for C-N.

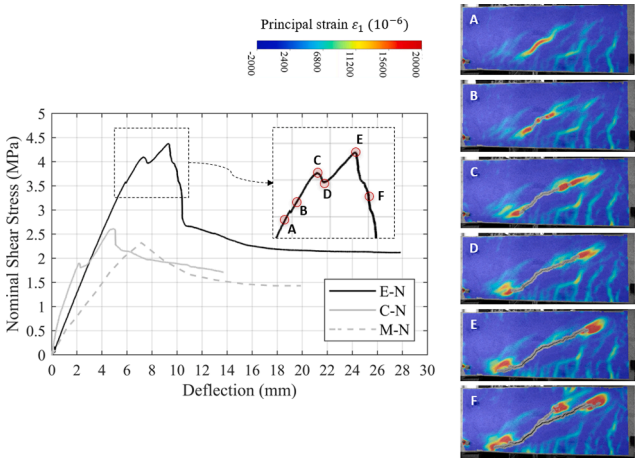

Fig. 12. Cracking patterns at selected load levels for E-N.

$$V_u = V_c + V_s = V_c + \sum_{1}^{n} V_{si} \tag{1}$$

where V_{si} is the force of i th stirrup leg and n represents the total number of transverse rebars crossing the critical shear crack. It should be noted that the Gauge 1 in Fig. 3(c) is installed in the region with screw threads outside. Therefore, when calculating the tensile force of stirrup leg at this position, the reduced nominal diameter of 10.4 mm should be used instead of 12 mm.

To measure the strain distribution along the full length of longitudinal reinforcement, strain gauges were also attached to these rebars. Steel rebars with diameter of 22 mm were used as top and bottom reinforcement, and a cavity of 8 mm in width and 4 mm in depth was made on their surface, as shown in Fig. 4(a). Strain gauges with length of 5 mm were attached in the cavity, which was also filled with silicon sealant, as shown in Fig. 4(b). As mentioned before, only half-span of the beam was equipped with such strain gauging system, and the other span was reinforced with dense stirrups to prevent shear failure. To enhance the anchorage of longitudinal rebars, steel plates with prefabricated-holes and a set of nuts were used to fix and anchor the rebar ends, as shown in Fig. 5. It should be mentioned that, since cavities were made inside stirrup legs and on the surface of longitudinal reinforcement, the actual cross-sectional area 95.10 mm^2 (stirrup leg) and 348.13 mm^2 (longitudinal reinforcement) should be used in the calculation of tensile reinforcement ratio, shear reinforcement ratio and yield strength.

2.3. Material preparation

The mixture composition of concrete, ECC and mortar used in this study is listed in Table 1. The maximum size of coarse aggregate for concrete is limited to 20 mm. For ECC, the short Polyvinyl Alcohol (PVA) fiber with length of 12 mm and diameter of 40 μm developed by Kuraray Co., Ltd. (type RECS15) is used for reinforcing the matrix. The tensile strength, Young's modulus and strain capacity of the PVA fiber is reported as 1560 MPa, 41 GPa and 6.5%, respectively, by the producer. To enhance the ductility and robustness of ECC, 20% of the fly ash is

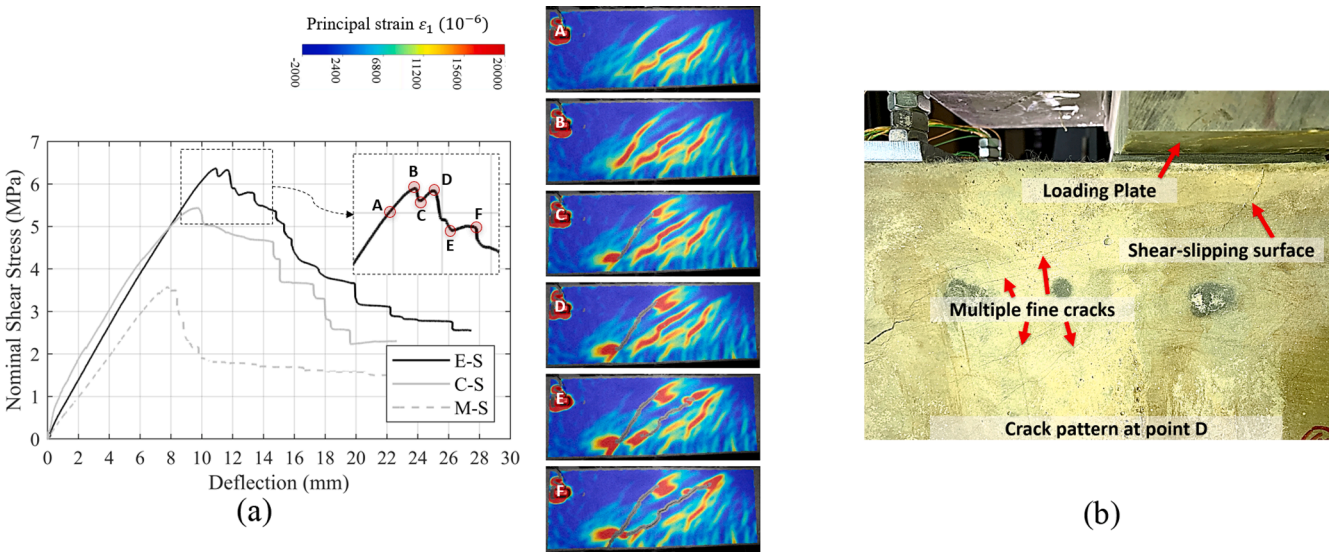

Fig. 13. Cracking patterns at selected load levels for E-S: (a) full-field strain map; (b) shear-slipping behaviour of ECC at peak load.

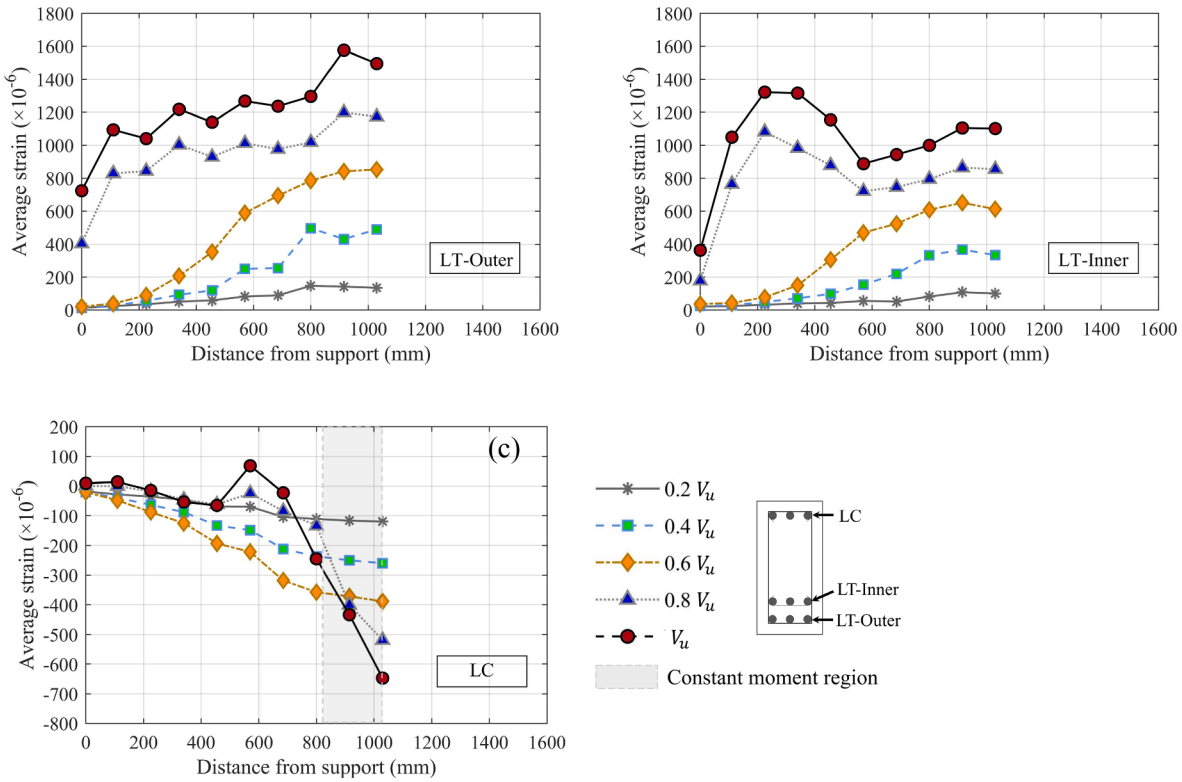

Fig. 14. Strain distribution along longitudinal rebars for concrete beam C-N: (a) outer row of tensile rebars; (b) inner row of tensile rebars; (c) compressive rebars.

replaced by light-weight cenosphere, which can help to lower the matrix toughness and homogenize its pore distribution [56]. The mortar used in this study has the same mix composition as ECC except the addition of PVA fibers.

Deformed steel bars with diameters of 12 mm and 22 mm were used as stirrups and longitudinal reinforcement respectively, with the yielding strength of 440 MPa and 635 MPa.

2.4. Test setup

Four-point bending test was adopted for all beam specimens, using a 3000 kN electro-hydraulic servo testing machine. The load was monotonically applied with a displacement control at a rate of 0.4 mm/minute. To keep the reaction at two supports equal to each other, a steel distributive beam was equipped between the loading cell and specimen with load applied at its mid-span. Three linear variable displacement transducers (LVDTs) were employed to monitor the mid-span deflection and settlement of two supports. Another two LVDTs are employed along the cross section of mid-span to detect its rotation during loading which would be induced by the asymmetry configuration of reinforcement, as illustrated in Fig. 6. A data logger was used to record the displacement and strain data from LVDTs and strain gauges with a frequency of 2 Hz. The three-dimensional Digital Image Correlation (3D-DIC) system PMLAB developed by Shao and He et al. [57–60] was utilized to detect

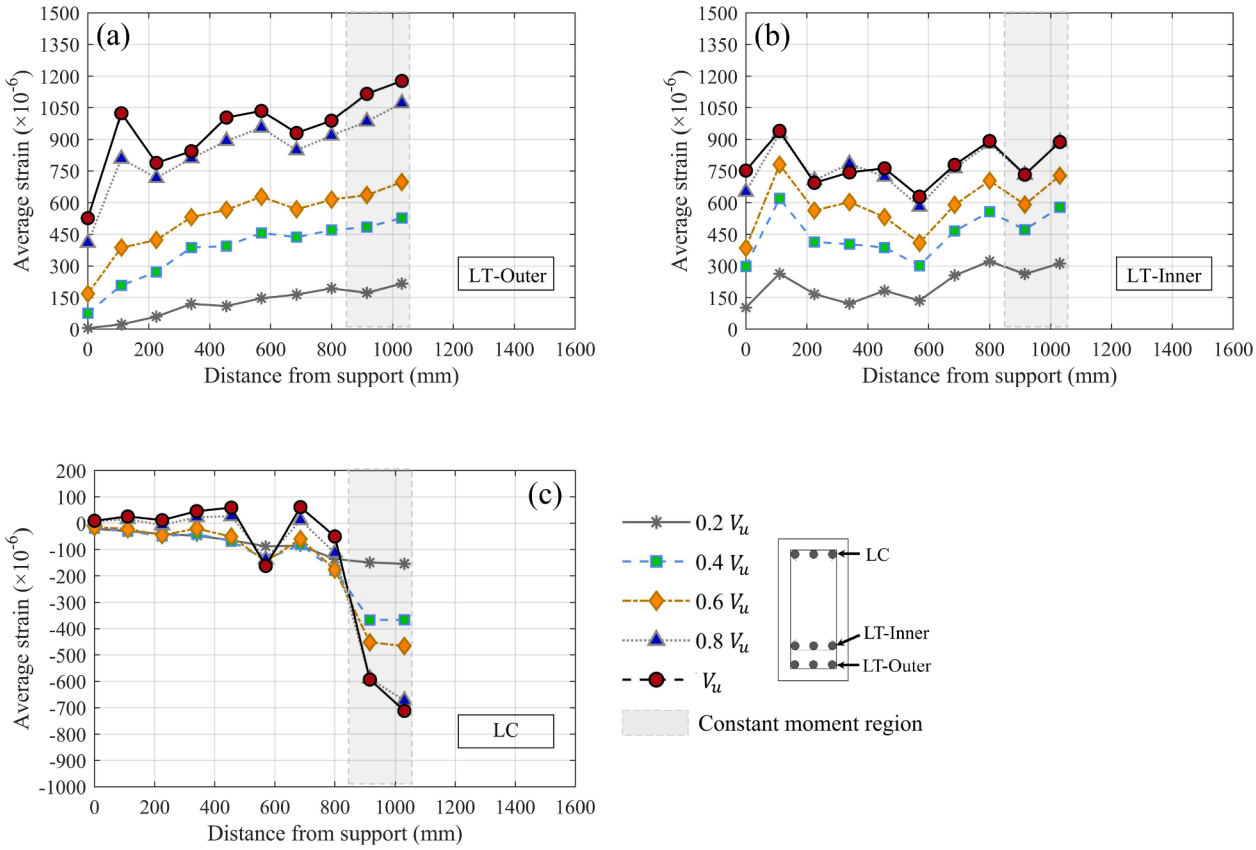

Fig. 15. Strain distribution along longitudinal rebars for mortar beam M−N: (a) outer row of tensile rebars; (b) inner row of tensile rebars; (c) compressive rebars.

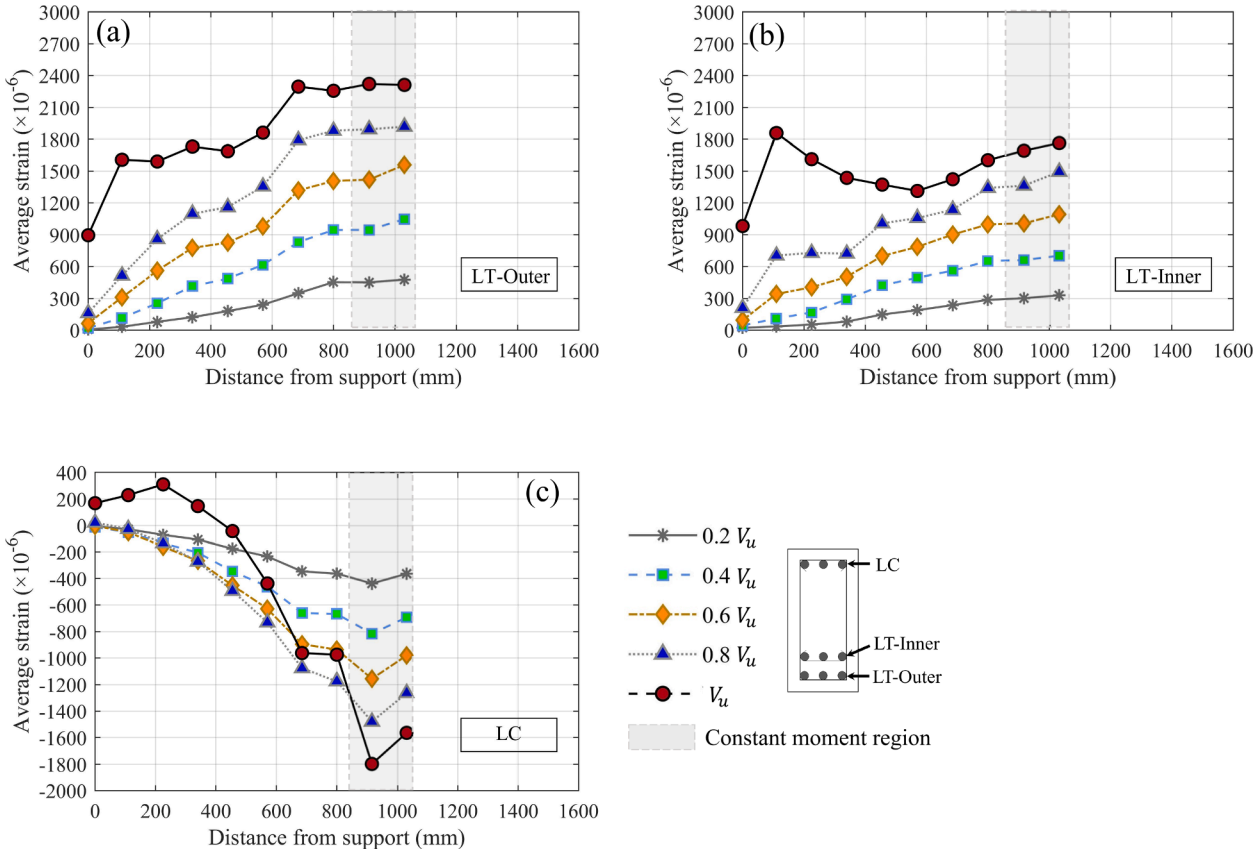

Fig. 16. Strain distribution along longitudinal rebars for ECC beam E-N: (a) outer row of tensile rebars; (b) inner row of tensile rebars; (c) compressive rebars.

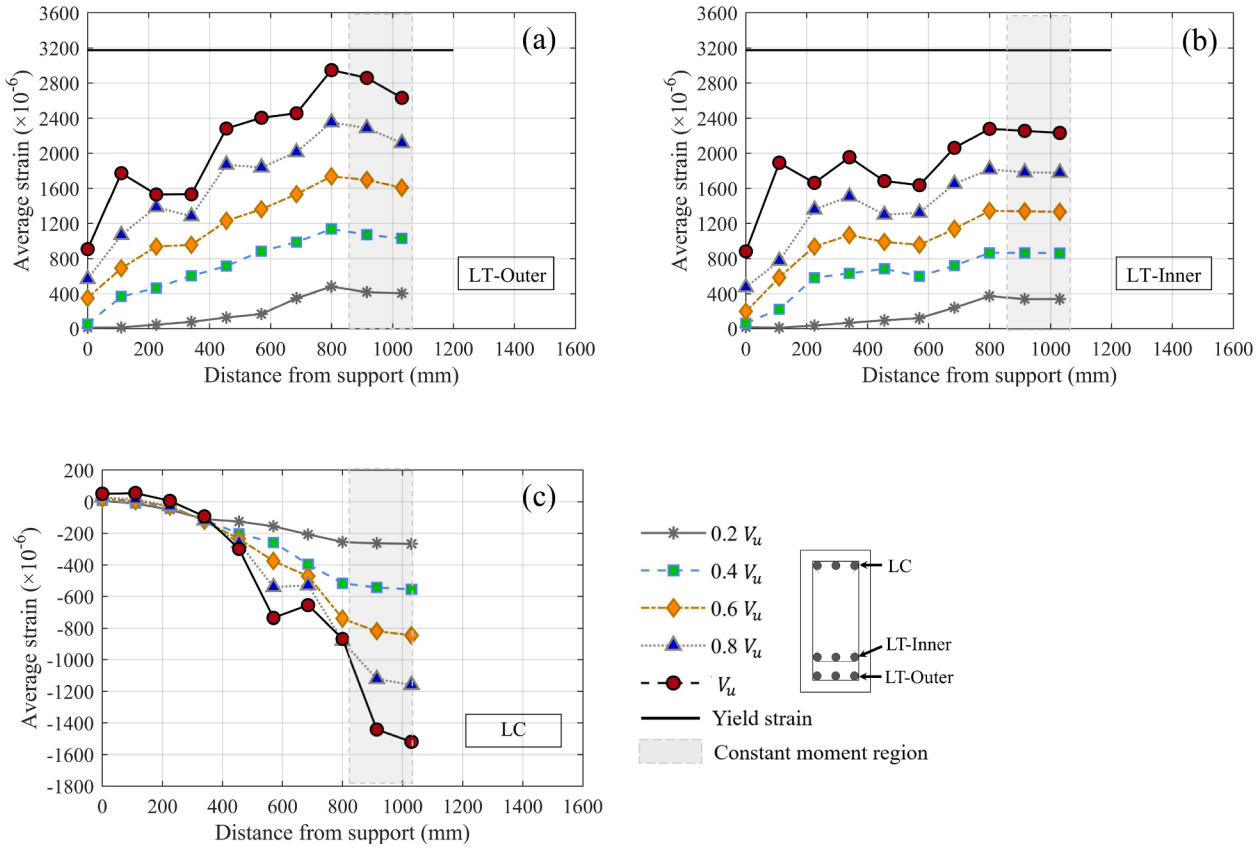

Fig. 17. Strain distribution along longitudinal rebars for concrete beam C-S: (a) outer row of tensile rebars; (b) inner row of tensile rebars; (c) compressive rebars.

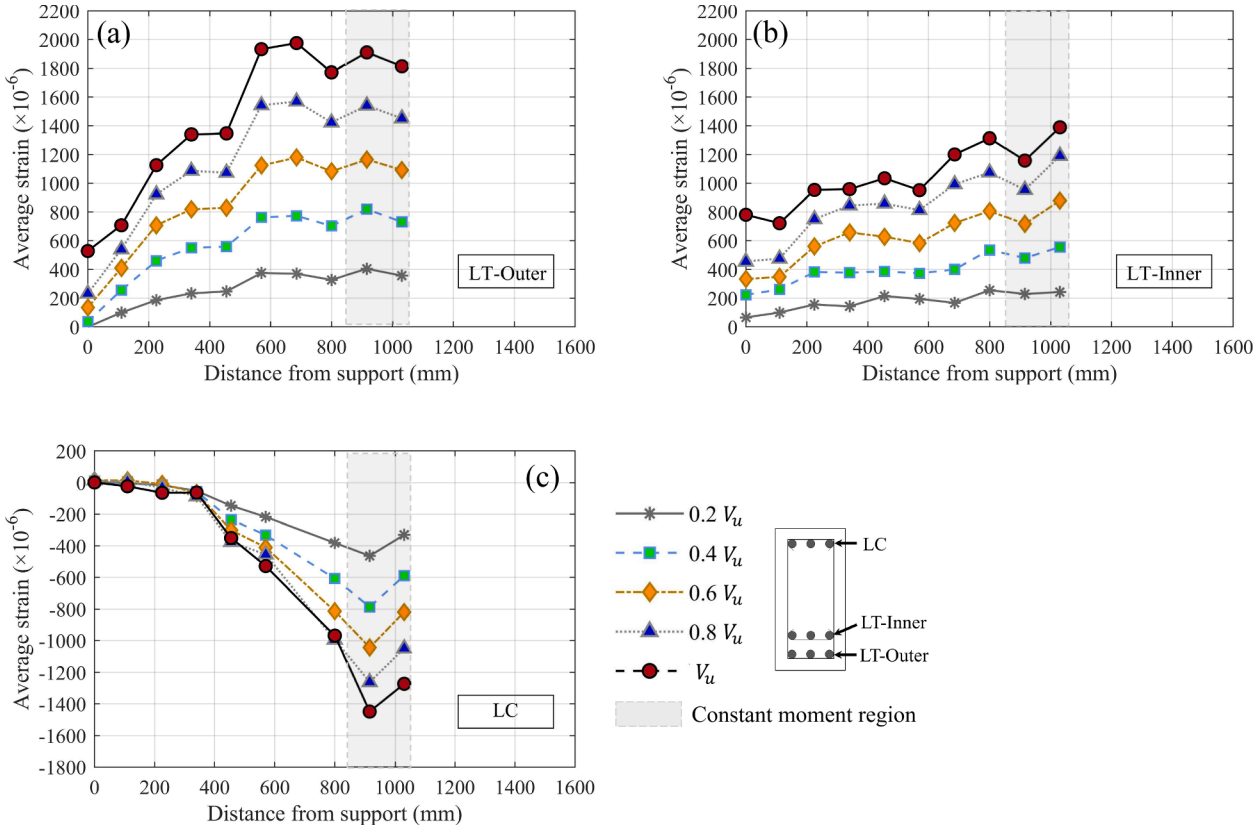

Fig. 18. Strain distribution along longitudinal rebars for concrete beam M–S: (a) outer row of tensile rebars; (b) inner row of tensile rebars; (c) compressive rebars.

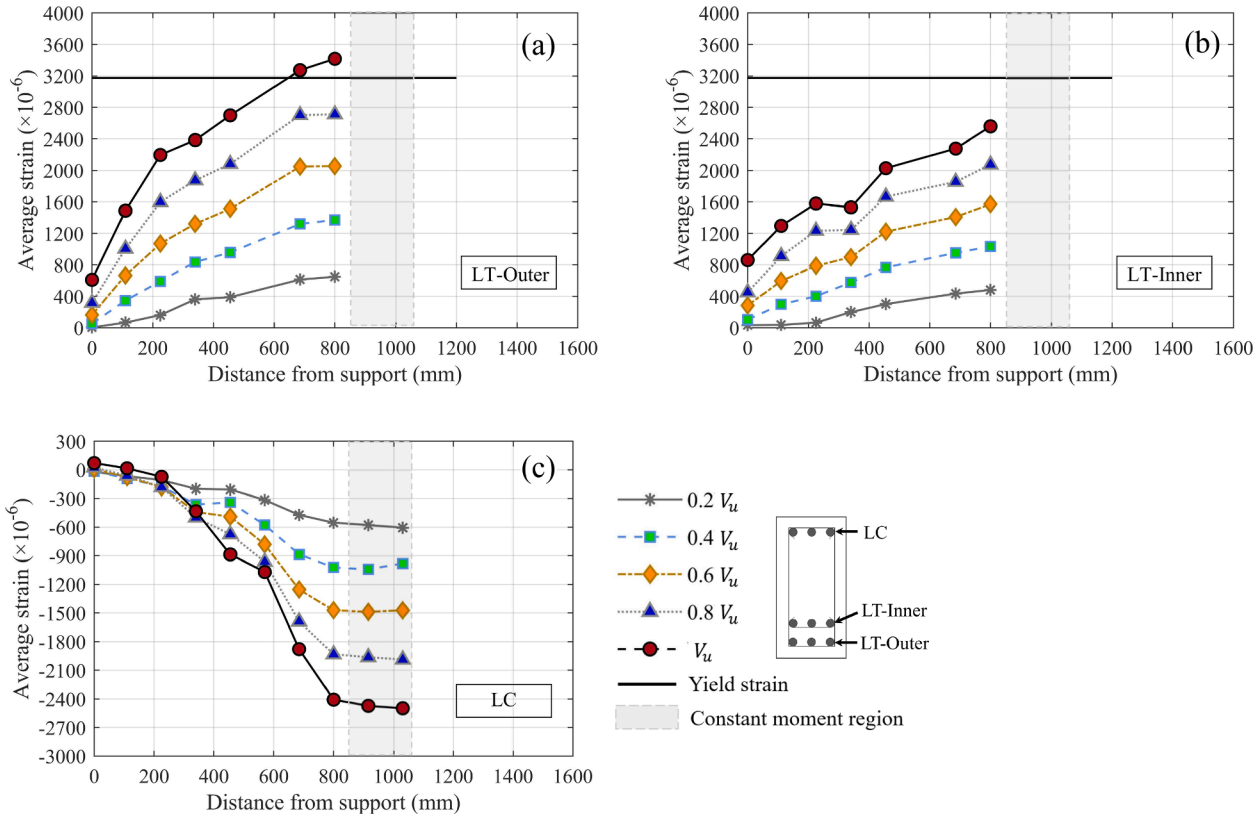

Fig. 19. Strain distribution along longitudinal rebars for concrete beam E-S: (a) outer row of tensile rebars; (b) inner row of tensile rebars; (c) compressive rebars.

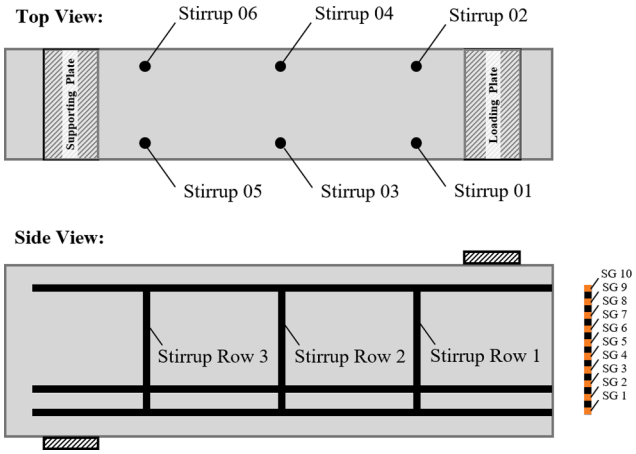

Fig. 20. Designation for stirrup legs and strain gauges (SGs) at different positions.

full-field deformation of beam surface.

3. Experimental results and discussion

3.1. Material tests

For each beam, at least six cylinders with diameter of 100 mm and height of 200 mm were prepared and tested under uniaxial compression at the same testing day. Besides, for each R/ECC beam, dumbbell-shaped specimens with a representative cross section of 15 mm × 30 mm were prepared for uniaxial tensile tests, following the standard test method provided by JC/T 2461–2018 and JSCE-08 [44,61]. Several cylinders were selected to measure the compressive stress–strain relationship for different matrices. The material test results, along with the shear capacity of the beams, are summarized in Table 2. Under uniaxial compression, the elastic modulus for concrete, ECC and mortar was tested to be 33.2 GPa, 21.5 GPa and 22.4 GPa, respectively and the corresponding Poisson's ratio was 0.20, 0.21, 0.23, respectively. The nominal tensile yield strength f_{ty} and ultimate tensile strength f_{tu} for ECC are also determined by tests and listed in Table 2 following their definitions in JSCE 08 [44]. Fig. 7a, 7b and 7c shows the stress–strain relationship under uniaxial compression and tension of selected ECC specimens and steel rebars.

3.2. Failure mode and shear force–deflection curves of beams

The shear force to deflection curves of beam specimens are exhibited in Fig. 8, and the post-peak crack patterns ($0.8V_u$ after the peak load) are shown in Fig. 9. Typical shear-compression failure was observed in all specimens, during which diagonal cracks formed in shear span and propagated to the support and loading plate, with load increasing. The peak load was achieved due to the crushing of matrix in the shear compression zone near loading plates.

Due to the absence of coarse aggregates, ECC and mortar would have a reduced elastic modulus and higher shrinkage compared to concrete, therefore obvious lower stiffness in reinforced ECC and mortar beams could be found at their initial loading stage, as shown in Fig. 8. However, this situation changed when first shear crack formed in concrete beam C-N at load of 125 kN. Significant decline of stiffness for the concrete beam occurred with rapid increase of deformation, but the counterpart ECC beam E-N could steadily sustain the shear force without sudden drop of member stiffness. When comparing the ECC and mortar beams, although they had similar elastic modulus, the R/ECC specimen exhibited an enhanced stiffness in the beginning, which highlights that the addition of PVA fibers in ECC could effectively mitigate the effect of shrinkage cracks on the stiffness of members. Comparing beams with and without stirrups, it was observed that the configuration of transverse

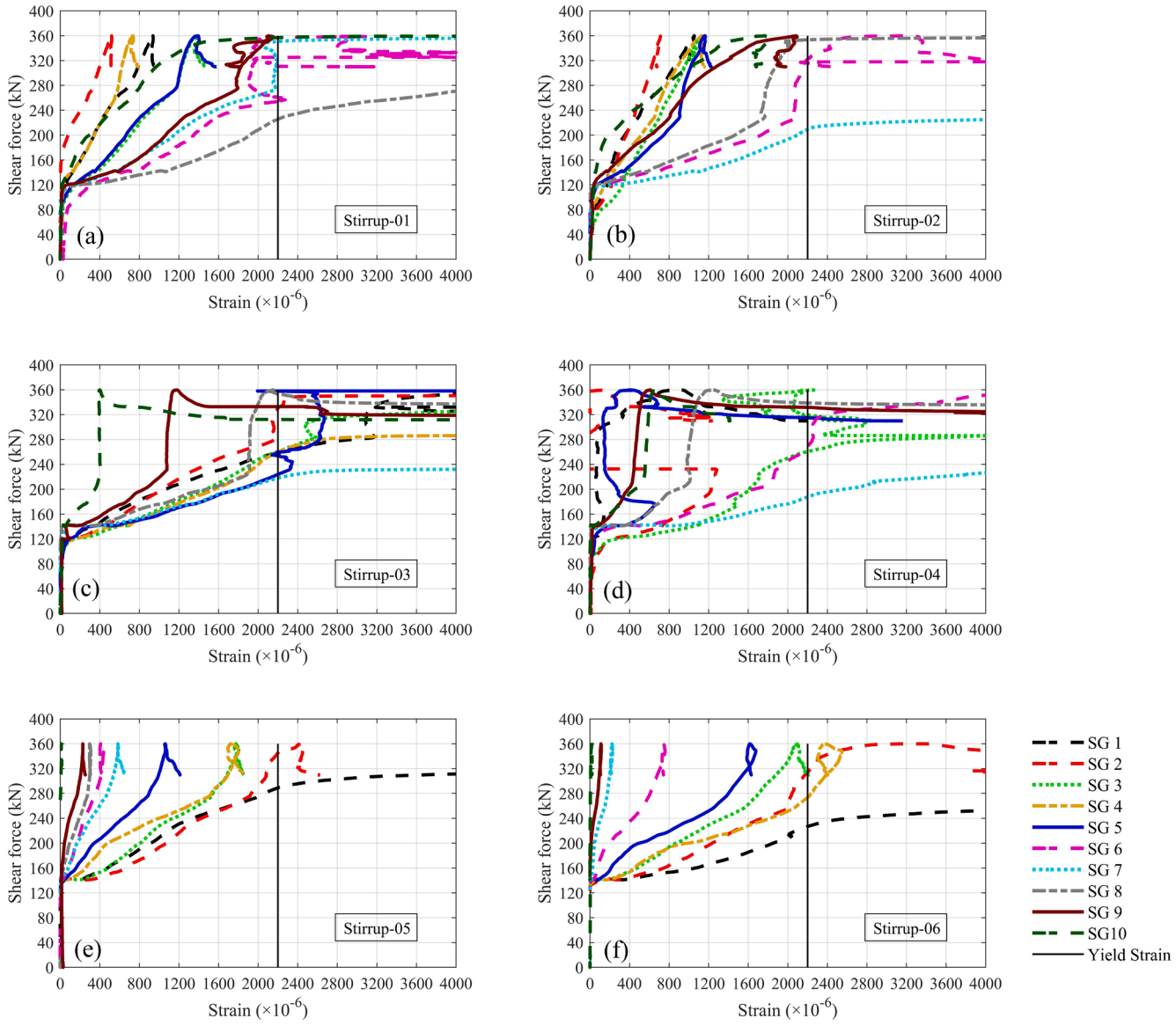

Fig. 21. Shear force versus strain in each stirrup leg for the concrete beam C-S (damaged strain gauges are not presented).

reinforcement would not influence their initial stiffness since the deformation mainly resulted from flexure at the onset of loading. However, after the development of shear crack, an enhanced post-cracking stiffness could be achieved by shear crack-restriction from these shear reinforcements.

3.3. Crack propagation and ultimate shear strength

With 3D-DIC system, the full-field strain spectrum could be illustrated, as shown in Fig. 10. The crack position can be linked with the region where high principle strains were identified. The average shear stress $v = \frac{V}{bd}$ is adopted when discussing the cracking behaviour at different load stage, where V is the shear force and b, d is the width and effective depth of the beam respectively.

3.3.1. Beam specimens without stirrups (C-N, M−N and E-N)

For beams without stirrups, flexural cracks were first found in pure bending region since it experiences the maximum bending moment. Different from ECC and mortar, the concrete beam C-N experienced a sudden but small drop of load at a shear stress v of approximately 1.9 MPa. The crack patterns of C-N at the critical locations over load-deformation response are shown in Fig. 11. At point A (v = 1.7 MPa), the extreme left flexural cracks changed its vertical orientation and started to rotate towards the loading plate, which could be named flexure-shear crack. When reaching point B (v = 1.9 MPa), the flexure-shear crack widened. After that, there was a load drop at point C with a crack clearly extending to both loading and supporting plates. With further increasing deflection, the stresses redistributed and new equilibrium of internal force was established. After point C (v = 1.8 MPa), the load did not decrease further and a secondary load-carrying stage followed, during which the load increased but stiffness reduced significantly. From point C (v = 1.8 MPa) to point E (v = 2.0 MPa), a splitting crack quickly formed along the longitudinal rebars, indicating the loss of rebar bonding and dowel action, and activating the arch action [62]. Finally, the RC beam without stirrup reached its ultimate shear carrying capacity due to crushing of concrete close to the loading plate, with a maximum average shear stress v = 2.6 MPa.

For the mortar beam M−N, the first shear crack was found at the shear stress v = 0.7 MPa, which was earlier than in RC beam. This crack propagated rapidly to the load and support points with very little load increase. Unlike with concrete beam where only one critical shear crack formed, more shear cracks were generated in the mortar beam before

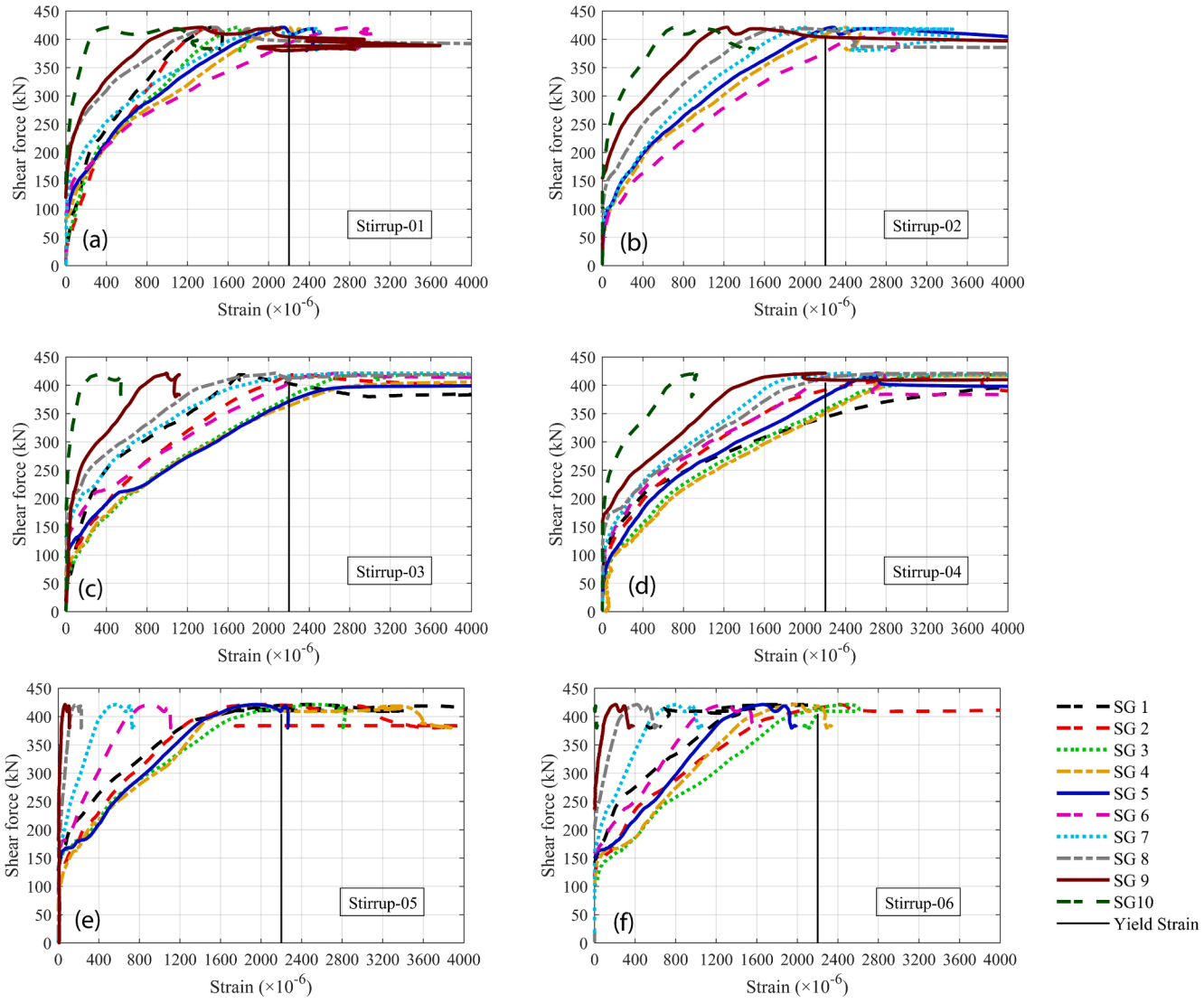

Fig. 22. Shear force versus strain in each stirrup leg for the ECC beam E-S (damaged strain gauges are not presented).

reaching its shear carrying capacity (Fig. 10). At the shear stress v = 2.3 MPa, due to the narrow shear compression zone, the mortar beam could not sustain anymore the load increase.

For the ECC specimen E-N, the first shear crack initiated from the mid-height of the beam section at around v = 1.5 MPa. Unlike sudden crack appearance and localization in RC beam, the shear crack in ECC exhibited more steady development. Until v = 3.5 MPa (Point A, Fig. 12), the localization of major shear crack in ECC was firstly observed. When shear stress reached around v = 3.6 MPa, a small load drop was observed, corresponding to the moment between point A and point B as illustrated in Fig. 12. As shown by the selected crack pattern, such fluctuation of load resulted from a sudden widening of the critical shear crack, probably accompanied with local fiber pull-out and/or rupturing. With further increase in load, the shear crack gradually and stably extended towards the loading and supporting plates. When the shear stress increased to v = 4.1 MPa, an obvious drop of load was found (corresponding to point C to D in Fig. 12), during which the shear resistance from fiber bridging across the critical shear crack was almost lost. Beyond point D, the beam sustained again the increasing shear force. This indicates that other shear transfer mechanism, like dowel action of tensile rebar and shear resistance from intact ECC matrix in compression zone, could still resist the further increase of load. The ultimate shear stress v = 4.4 MPa was reached along with compressive failure of ECC underneath the loading plate, which was 1.7 and 1.9 times higher than that of concrete and mortar reference beams.

3.3.2. *Beam specimens with stirrups (C-S, M−S and E-S)*

When reinforced with stirrups, all three beam specimens exhibited remarkably increased shear strengths and denser crack pattern. For the concrete beam with stirrups C-S, the first shear crack appeared at v = 1.8 MPa, which was almost the same as that of C-N. However, unlike in C-N beam, C-S beam, did not experience any drop of load when initial shear crack happened. Stirrups could be activated immediately to undertake the increasing load upon the formation of shear cracks. Instead of only one major shear crack, more shear cracks formed during load increase. Besides, no obvious splitting crack was found along longitudinal tensile reinforcement, signifying an enhanced dowel action due to effective crack restriction from transverse reinforcement. When the shear stress reached v = 5.4 MPa, the beam could not sustain further increase of load due to the crushing of concrete in compression, achieving nearly twice as high shear strength compared to the specimen without stirrups. For the mortar beam M−S with stirrups, more saturated crack pattern was observed compared with the concrete ones. However, although reinforced with same number of stirrups, the ultimate shear strength of mortar beam was only 67% that of concrete. This might be attributed to the absence of aggregate interlock in mortar

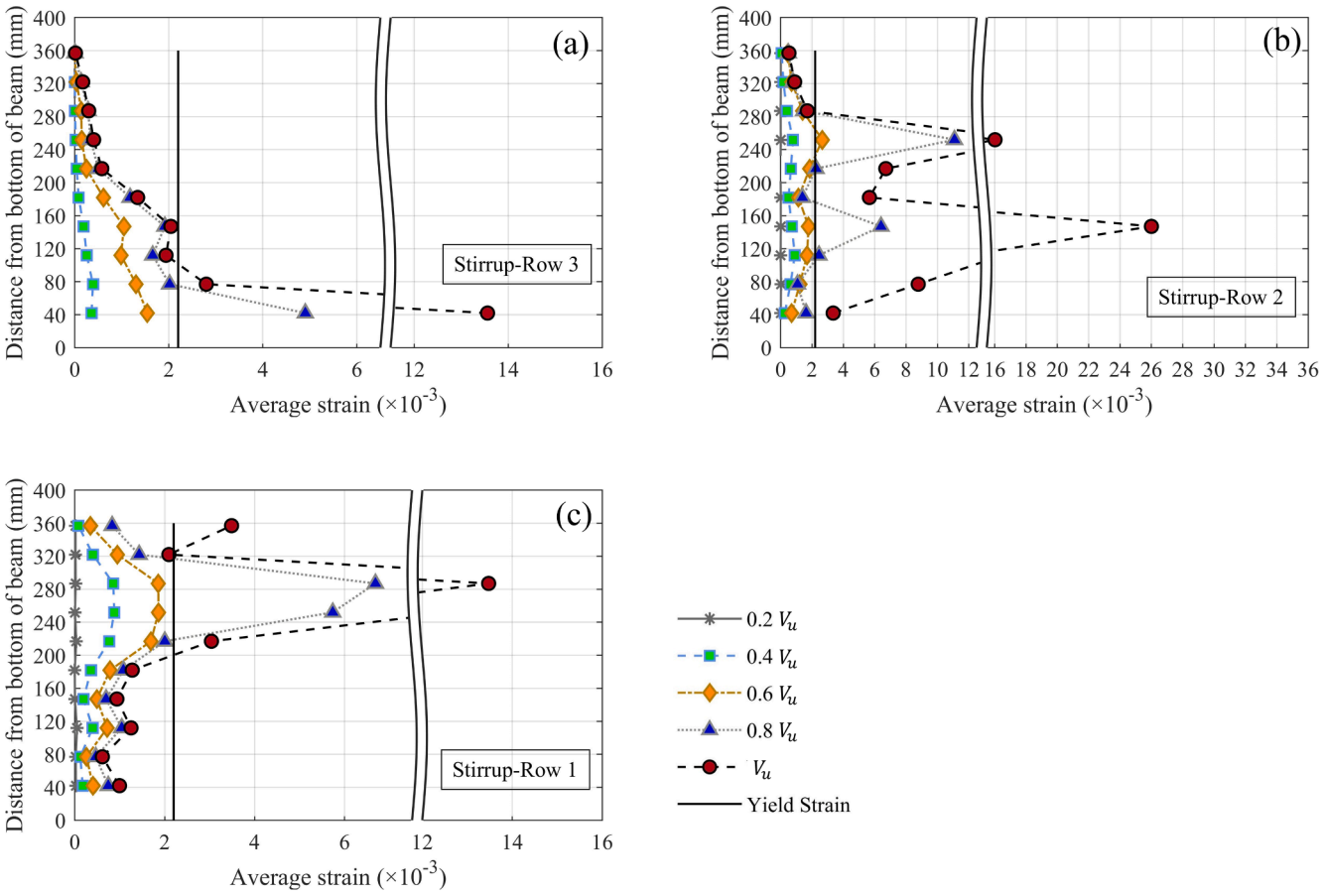

Fig. 23. Strain distribution along stirrups for concrete beam C-S: (a) stirrup near support; (b) stirrup in the middle of shear span; (c) stirrup near loading plate.

beams.

For the ECC beam with stirrups E-S, the shear crack was first observed at shear stress $v = 1.2$ MPa, which was a bit earlier than the concrete ones. Compared with E-N, more diagonal cracks could be found during the loading process. Similarly as observed in C-S, the localization of critical shear crack was also postponed compared to E-N. As Fig. 13(a) shows, until the first peak load was reached (point B, $v = 6.4$ MPa), no visible major crack was observed. From point B to point C, a small drop of load happened due to the sudden widening and localization of one shear crack. After that, a new equilibrium of internal force was established and the shear stress could increase again to $v = 6.3$ MPa (point D). At this moment, the major shear crack suddenly widened, probably accompanied with fiber pull-out and/or rupture, resulting in a rapid drop of load from point D to point E. The crack extended to the loading and supporting points, causing a reduced height of shear-compression zone. At the same time, the shear-slipping happened in ECC matrix underneath the loading plate, as shown in Fig. 13(b). The ECC compression zone could not undertake the increasing load any more, which led to the ultimate failure of the beam. Compared with the reference mortar beam M−S, the shear carrying capacity was about 80% higher due to addition of PVA fibers. However, the shear strength gap between ECC and concrete beam was narrowed when reinforcing with certain number of stirrups. It showed that only 17% increase of shear strength was obtained when substituting concrete with ECC, revealing an altered shear transfer mechanism and contribution of different components when stirrups were incorporated.

3.4. Strain in longitudinal reinforcement

The strain distribution along longitudinal reinforcement for all beams under selected load levels is illustrated from Figs. 14-19. For each strain gauging position, the strains of three rebars at the same level are averaged and shown. The relative position of rebars and strain gauges can be found in Fig. 4 and Fig. 9. It should be noted that the strain gauges 9 and 10 were installed within the pure bending region of constant moment, which should exhibit the same strain value before cracking.

For beams without stirrups, due to a higher load carrying capacity, the longitudinal rebars of ECC specimen E-N exhibited higher strain than C-N and M−N at peak loading level. Just before cracking, the strain distribution in longitudinal reinforcement was approximately equal in the constant moment region and linear in the constant shear stress region, which was consistent with the moment diagram. However, when the critical shear crack formed, a strain concentration was found for all beams in tensile rebars at the location where the shear crack crossed the rebar. When referring to tensile rebars at inner layer, it is interesting to find a sharp increase of tensile strain near the support, as shown in Fig. 14(b), Fig. 15(b) and Fig. 16(b). It is known as tension-shifting effect due to the sudden reduced tensile stress along the inclined shear cracking surface [63]. Besides, due to the formation of splitting crack and rebar debonding, the strains of tensile rebars at the support were non-zero, which justified a demand of effective anchoring to prevent premature anchorage failure under shear. Furthermore, it also revealed the degradation of beam action and the formation of strut-and-tie [62]. For longitudinal compressive rebars, around the peak load, some strain gauges exhibited positive values which meant tensile stress was detected. This tensile stress was induced by the buckling of top rebars, which caused bending of rebar and tension to be found on one side of the rebar section. However, such buckling was significantly postponed in the ECC beam E-N and could be observed only in the last loading step. This could be possibly attributed to the better confinement effect of fiber reinforced matrix compared with concrete and mortar.

When reinforcing with stirrups, the tension-shifting effect was

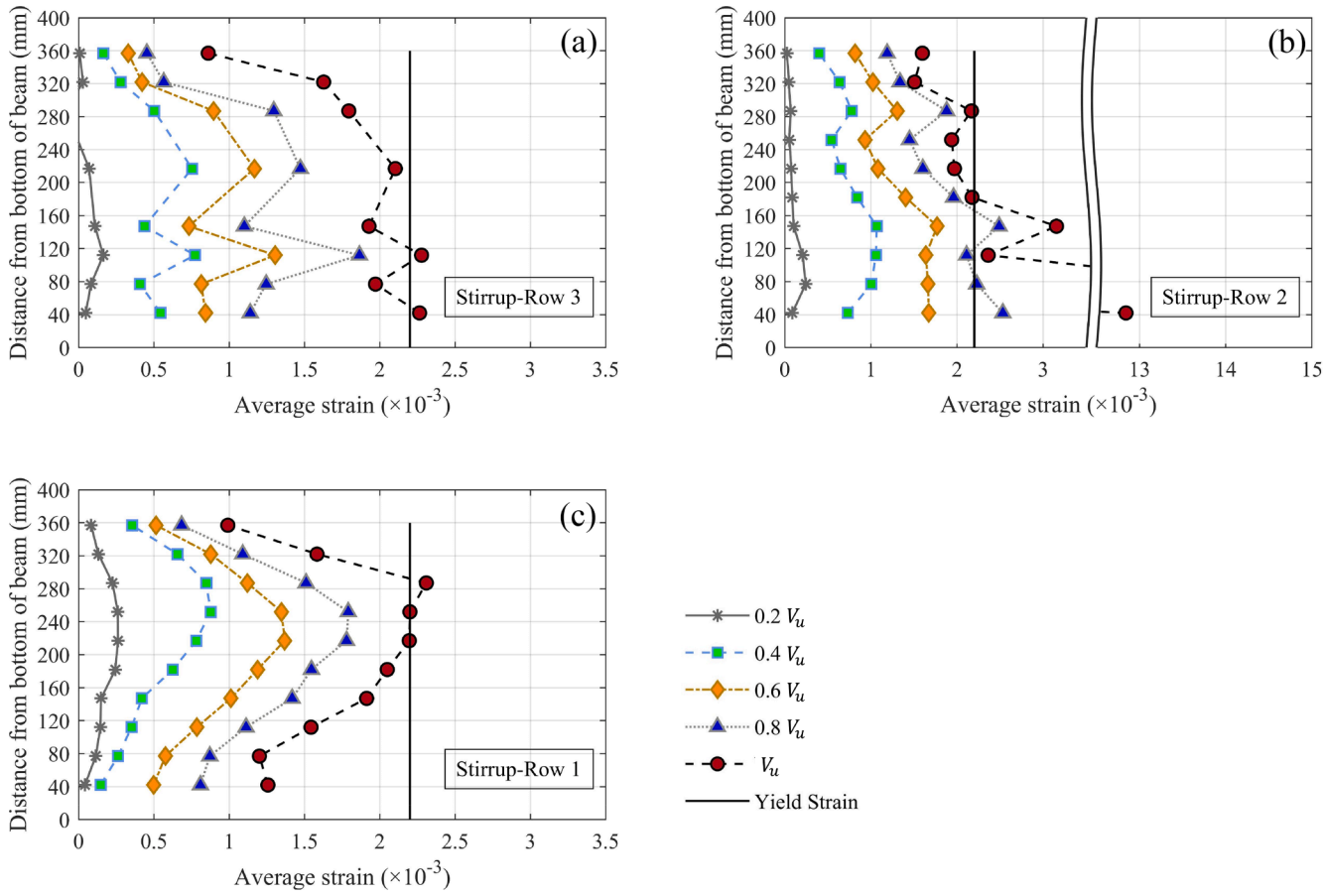

Fig. 24. Strain distribution along stirrups for mortar beam M−S: (a) stirrup near support; (b) stirrup in the middle of shear span; (c) stirrup near loading plate.

delayed for all three beams. The configuration of stirrups could effectively restrict the development of shear-splitting cracks along longitudinal reinforcement, bringing significant enhancement of bonding between matrix and rebars [64]. Besides, the tensile strain was not observed in top compressive rebars since closed stirrups could also restrict them from bulking. For the E-S beam, yielding of tensile rebar occurred at peak load, as shown in Fig. 19(a) (the strains along constant moment region were lost due to data logger error). However, and the shear failure is still critical due to shear crack localization and shear-slipping of ECC matrix underneath the loading plate prior to flexure, as depicted in Fig. 13. By incorporating the analytical method for evaluating flexure behavior of R/ECC beam proposed by [65], the flexure carrying capacity of E-S is calculated to be around 1050 kN, with a corresponding shear force of 525 kN. Compared to the ultimate shear force of 421.4 kN, the beam E-S was still far from its flexural strength when ultimate failure happened, which proved again that its ultimate strength is controlled by shear.

3.5. Strain in transverse reinforcement

Fig. 20 illustrates the distribution of stirrup legs and their strain gauges (SG) in the beams. Fig. 21 and Fig. 22 depict the shear force versus strain in each stirrup leg for concrete and ECC beams with stirrups.

For the concrete beam, before the shear crack occurred, quite limited strain could be observed in stirrup legs (Fig. 21). During this stage, almost all the shear force was resisted by the concrete part V_c. Upon the shear crack forming at 120 kN, the transverse rebars were activated, indicating an increased contribution of shear resistance by V_s. After that, most of the stirrup strain increased at a certain rate until the yielding. As illustrated in Fig. 21(b), when the shear force reached around 220 kN, the yielding of SG7 in stirrup 2 occurred. After this moment, the strain of SG7 increased at a higher rate but the strain growth at other position was slowed down, which revealed the widening and localization of the critical shear crack. After the peak load, most of the stirrup strain stopped increasing due to reduced external load. However, the strain gauges where the critical shear crack intersected exhibited rapidly increasing tensile strain despite the dropping load, which meant a continuous growth of crack width and constant shear resistance from V_s with the increasing deformation. It was also observed that the stirrup strain in front and back legs would not be the same during loading due to the three-dimensional nature of cracking surface. Therefore, assuming a fixed shear cracking path for attaching strain gauges before experiments would lead to inaccurate and unreliable estimation of V_s.

Different from brittle fracture in concrete, the shear cracks generated and propagated quite mildly in the ECC specimen E-S, which could also be evaluated by the strain development in stirrups. Before the first shear crack observed at about 80 kN, very small tensile strain in stirrup legs could be detected, as shown in Fig. 22. However, unlike an obvious turning point in concrete and mortar after shear cracking, the stirrup strain increased gradually at an accelerated rate. The stirrups in concrete and mortar firstly yielded at a shear force of 190 kN and 170 kN, however, the yielding of stirrups in ECC was retarded a lot to 350 kN due to synergistic deformation between ECC and steel rebars. The stirrup strain in ECC kept increasing in a stable manner until the shear force reached around 95% the maximum shear carrying capacity, at which moment the shear crack localized with fiber pulling out and rupturing. After that, the stirrup strain grew rapidly with very little increase in the load, which marked the failure of beam.

The strain distribution along stirrups under selected loading levels for all three beams is shown from Fig. 23 to Fig. 25, and the average strain of two stirrup legs in front and back is plotted. No matter for

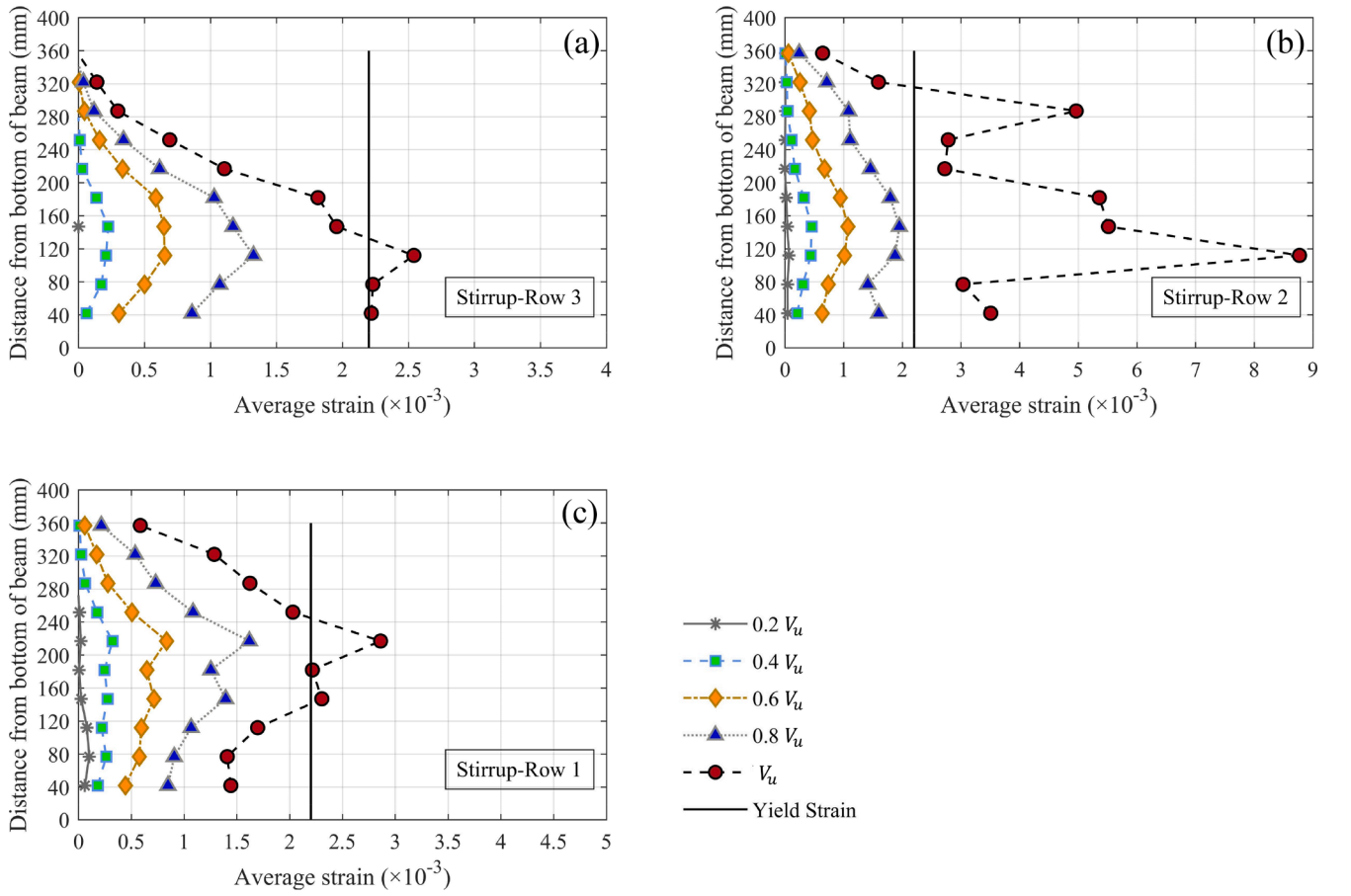

Fig. 25. Strain distribution along stirrups for mortar beam E-S: (a) stirrup near support; (b) stirrup in the middle of shear span; (c) stirrup near loading plate.

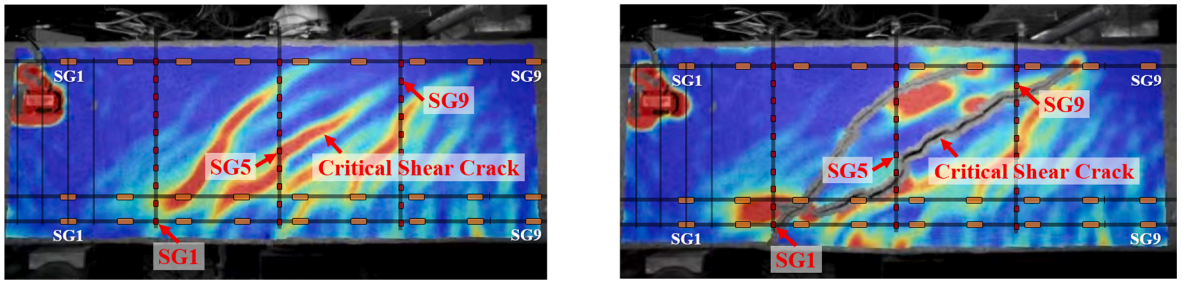

Fig. 26. Crack pattern for the ECC beam E-S: (a) at peak load; (b) at $0.8V_u$ after peak load.

concrete, mortar or ECC, the strains along stirrup legs in all beams were not uniform because of the bond between stirrups and matrix. When comparing stirrup strain distribution in Figs. 23-25 with the crack patterns in Fig. 10, it was found that the peak strain of stirrups happened where the shear crack was crossed. Since the diagonal shear crack would cross the stirrup legs at any height, the maximum strain along stirrups was not always at the mid-height of beam, so measuring the strain at mid-height of stirrups could not give their true shear resisting contribution. For the mortar beam M−S, it could be observed that the stirrups were activated earlier than other two beams. Owing to the superior deformation capacity and crack control of ECC material, stirrups in E-S exhibited lower strain distributions at peak load compared with the concrete reference beam. When the peak load was reached, the critical shear crack formed and crossed the stirrup row 1, stirrup row 2 and stirrup row 3 at SG9, SG5 and SG1 separately in the ECC beam E-S, as shown in Fig. 26. When referring to the stirrup strain exhibited in Fig. 25 (c), the strain gauge SG9 in stirrup row 1 detected a strain of only 1285 με, which was far from yielding (2200 με). It indicated that not all the stirrups crossed by critical shear crack would yield at the onset of shear strength, and calculating V_s with yielding strength for all stirrups intersecting the critical shear crack would lead to unsafe prediction of shear strengths.

3.6. Variation in V_s and V_c

With stirrup strain obtained from the strain measuring system, V_s and V_c can be calculated. In the following evaluation, the critical shear crack with maximum crack width at peak load would be analyzed, and the stirrup strain gauges intersected by the critical shear crack were selected for calculating V_s, as marked in Fig. 9. With the measured strains and stress–strain relationship obtained from rebar tensile tests in Fig. 7(c), the transverse force for each stirrup along the critical shear crack could be calculated. Then, V_s can be determined by summing up all these transverse forces, and V_c can be derived by subtracting V_s from V

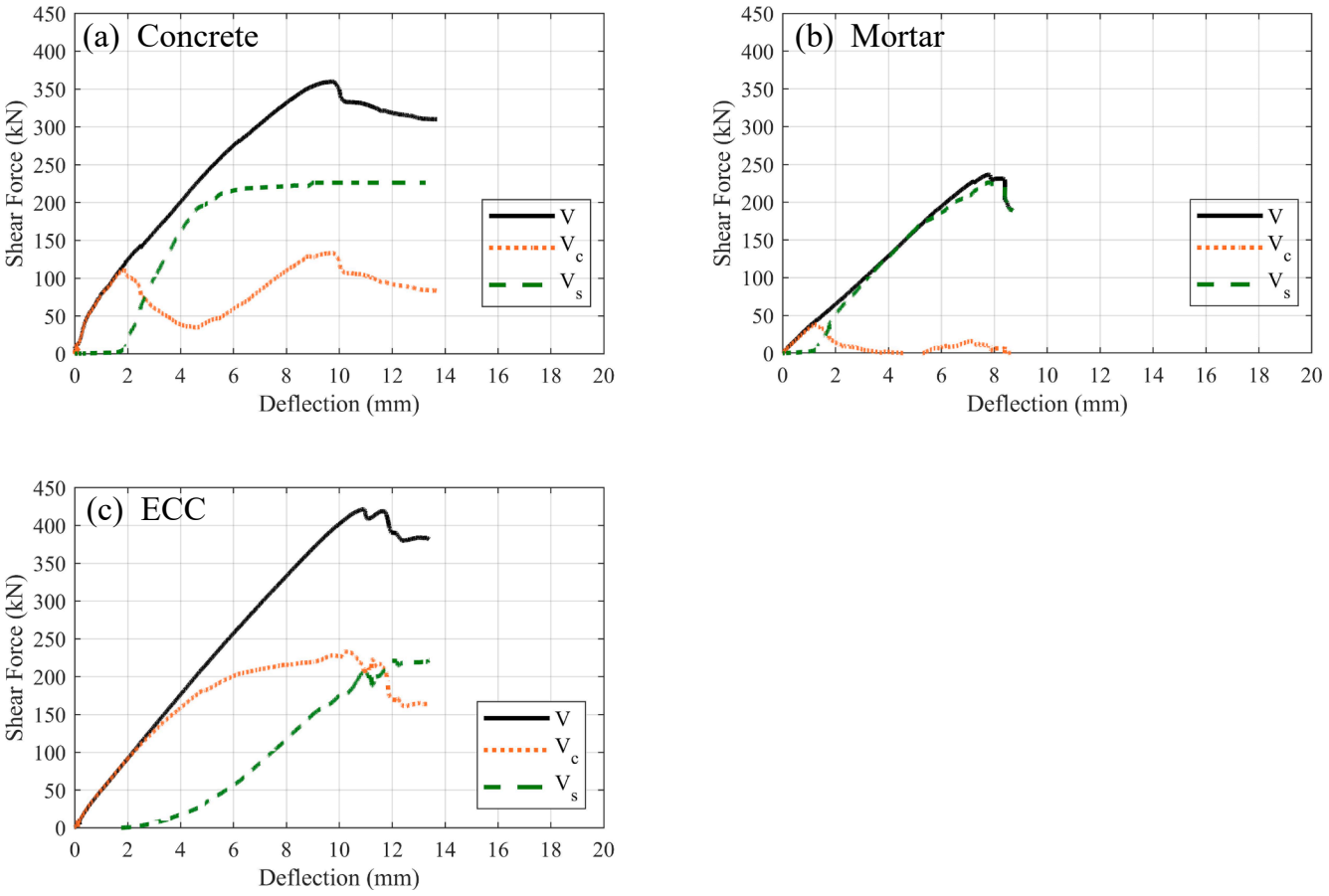

Fig. 27. Variation in V_s and V_c against deflection for the beam: (a) C-S; (b) M−S; (c) E-S.

following Eq. (1). The variations in V_s and V_c against deflection for the beam C-S, M−S and E-S are illustrated in Fig. 27.

For the concrete beam C-S, almost all shear force was resisted by concrete V_c until the first shear crack formed. After that, the stirrups were fully activated and a quick increase of V_s was observed then. Meanwhile, a continuous drop of V_c was observed with crack widening and propagating, until stirrups started to yield at the deflection of 4.5 mm. Afterwards, the internal redistribution of stress occurred in concrete and a new equilibrium was achieved, resulting in a secondary growth of V_c. When V_c reached around 133 kN, which was somewhat higher than the first shear cracking load, the beam could not take the increasing shear force anymore. The ultimate shear failure happened due to the crushing of concrete in shear compression zone, and stirrups contributed around 70% to total capacity. When referring to the mortar beam M−S, the stirrups were activated quite early at a shear force of 37 kN due to premature formation of shear crack. After that, the V_c dropped rapidly and even to zero due to the absence of aggregate interlocking. The shear force was almost solely taken by the steel reinforcement. When the peak load was reached, the matrix contribution V_c only accounted for about 6.3% of the total shear force, revealing the poor damage tolerance of mortar without fiber reinforcement.

As depicted in Fig. 27(c), the activation of V_s in ECC was not really linear with shear force, like that in concrete and mortar, which delayed yielding of the stirrup. Without any resistance drop like in concrete and mortar, the shear resistance of ECC matrix kept increasing until the ultimate shear strength was reached, and the final failure was attributed to the shear-compression failure of ECC matrix beneath the loading plate. As mentioned before, it was found that not all stirrups which intersected with shear crack yielded at peak load, which indicates that superposition of yielding force of stirrups that intersects with diagonal crack would overestimate the shear contribution from transverse reinforcement.

Overall, the V_c of ECC beam E-S was about 1.9 times that of concrete beam C-S, but 16% reduction in V_s at peak load was found due to the incomplete yielding of stirrups crossing the critical shear crack. As a result, the total shear carrying capacity of the ECC beam E-S is only 13% higher than that of the concrete beam C-S. Nevertheless, until the peak load was reached, no obvious opening crack was found in the ECC beam, which revealed significantly smaller crack width than that of concrete and mortar under the same load level. The future research will focus on more detailed analysis of crack width kinetics based on DIC.

4. Conclusion

To individually evaluate the shear transfer mechanism and contribution from transverse reinforcement V_s and matrix V_c in reinforced structural beams, a well-designed experimental methodology is adopted in this work. Stirrup legs are cut into two halves and strain gauges are continuously installed inside, by which the continuous distribution of strain can be detected without disturbing the bonding between rebar and matrix. Then the V_s can be determined by the stirrup strain where shear crack crossed, and V_c can be calculated by subtracting V_s from the total shear force. A total of six reinforced beams incorporating different matrix (traditional concrete, mortar and ECC) were tested under four-point bending, and following conclusions can be drawn:

- The strain gauging system in this work was proved to be effective, and it could identify the development and variation of V_c and V_s throughout the whole loading process.
- Shear compression failure was found for all tested beam specimens with crushing of matrix in compression zone. Unlike sudden and rapid shear crack propagation in reinforced concrete and mortar

beams, steady and multi-cracking behavior was observed in ECC beams.

- For all samples, R/ECC, RC or R/mortar, V_c was found not constant after first shear cracking. For the RC beam, the V_c experienced a significant degradation after the shear crack appeared. When the stirrups started yielding, V_c increased again to around the initial cracking value. However, for the R/ECC beam, V_c kept increasing after shear crack happened until the ultimate shear failure, exhibiting 90% increase when compared with the RC ones. When removing addition of fibers, V_c in the R/mortar beam was almost lost after the formation of shear crack, although mortar had a similar compressive strength as concrete and ECC. This signifies the aggregate interlock contribution in shear resistance.
- The maximum strain along stirrups was found to be coincident with the location where critical shear crack crossed. The strain in front and back legs of stirrup was observed to be different due to 3D nature of shear cracking surface. Besides, stirrups crossed by shear crack did not always yield when ultimate shear strength was reached. Therefore, assuming yielding for all the stirrups along shear cracking path would lead to overestimation on V_s.
- Significant tension-shifting effect along longitudinal reinforcement was found for all the beams without stirrups after the formation of shear cracks. The non-zero strain in tensile rebars at supporting points revealed the demand of effective anchorage. Besides, configuration of transverse reinforcement could restrict the compressive rebars from buckling.
- The shear strength of R/ECC without stirrups was found to be 170% that of the reference concrete beam. However, when reinforced with stirrups ($\rho_t = 0.38\%$), the shear strength of R/ECC beam was found only 13% higher than that of concrete ones, which resulted from incomplete yielding of stirrups at ultimate shear failure. It revealed that strengthening the shear strength for structural members by substituting concrete with ECC would not be an economic and efficient way if the beams are reinforced with stirrups. However, for those structural members which could not be configured with transverse reinforcement like slabs, R/ECC would be a good alternative for enhancing their shear carrying capacity.

CRediT authorship contribution statement

Dawei Gu: Conceptualization, Methodology, Writing – original draft, Project administration. **Jinlong Pan:** Conceptualization, Supervision, Writing – review & editing. **Shozab Mustafa:** Writing – review & editing. **Yitao Huang:** Writing – review & editing. **Mladena Luković:** Supervision, Writing – review & editing.

Declaration of Competing Interest

The authors declare that they have no known competing financial interests or personal relationships that could have appeared to influence the work reported in this paper.

Acknowledgement

The work is financially supported by the National Natural Science Foundation of China (No. 51778131).

References

[1] Li VC, Leung CKY. Steady state and multiple cracking of short random fiber composites. J Eng Mech 1992;118(11):2246–64.
[2] Wang SX. Micromechanics based matrix design for engineered cementitious composites. University of Michigan; 2005.
[3] Fischer G, Li VC. Deformation behavior of fiber-reinforced polymer reinforced engineered cementitious composite (ECC) flexural, members under reversed cyclic loading conditions. ACI Struct J 2003;100:25–35.
[4] Hou L, Xu R, Chen Da, Xu S, Aslani F. Seismic behavior of reinforced engineered cementitious composite members and reinforced concrete/engineered cementitious composite members: A review. Structural Concrete 2020;21(1):199–219.
[5] Ma H, Yi C, Wu C. Review and outlook on durability of engineered cementitious composite (ECC). Constr Build Mater 2021;287(2):122719.
[6] Ahmaran M, Li VC. Durability properties of micro-cracked ECC containing high volumes fly ash. Cem Concr Res 2009;39(11):1033–43.
[7] Sahmaran M, Li VC, Andrade C. Corrosion resistance performance of steel-reinforced engineered cementitious composite beams. ACI Mater J 2008;105(3):243–50.
[8] Wang ZB, Sun P, Zuo JP, Liu C, Han YD, Zhang ZS. Long-term properties and microstructure change of engineered cementitious composites subjected to high sulfate coal mine water in drying-wetting cycles. Mater Des 2021;203(2):109610.
[9] Yun ML, Li VC. Durable repair of aged infrastructures using trapping mechanism of engineered cementitious composites. Cem Concr Compos 1997;19(4):373–85.
[10] Fukuyama H. Application of high performance fiber reinforced cementitious composites for damage mitigation of building structures case study on damage mitigation of RC buildings with soft first story. J Adv Concr Technol 2006;4(1):35–44.
[11] Maruta M, Kanda T, Nagai S, Yamamoto Y. New high-rise RC structure using pre-cast ECC coupling beam. Concrete Journal 2005;43(11):18–26.
[12] Fischer G. Application of engineered cementitious composites (ECC) in prefabricated modular housing. ACI Special Publication 2010;268:17–28.
[13] Lepech MD, Li VC. Application of ECC for bridge deck link slabs. Mater Struct 2009;42(9):1185–95.
[14] Zhang J, Wang ZB, Ju XC. Application of ductile fiber reinforced cementitious composite in jointless concrete pavements. Compos B Eng 2013;50:224–31.
[15] Zhang R, Matsumoto K, Hirata T, Ishizeki Y, Niwa J. Application of PP-ECC in beam–column joint connections of rigid-framed railway bridges to reduce transverse reinforcements. Eng Struct 2015;86:146–56.
[16] Müller S, Mechtcherine V. Use of strain-hardening cement-based composites (SHCC) in real scale applications. Dordrecht, Netherlands: International Conference on Strain-hardening Cement-based Composites 2018;15:690–700.
[17] Ritter W. Dir bauweise Hennebique. Schweizerische Bauseitung 1899;33(7):59–61.
[18] Mörsch E. Der Eisenbetonbau-Seine Theorie und Anwendung. V.1 Part 1. Wittwer, Stuttgart; 1920.
[19] Mörsch E. Der Eisenbetonbau-Seine Theorie und Anwendung. V.1 Part 2. Wittwer, Stuttgart; 1922.
[20] Vecchio FJ, Collins MP. The modified compression-field theory for reinforced concrete elements subjected to shear. ACI Journal 1986;83(2):219–31.
[21] Vecchio FJ, Collins MP. Predicting the response of reinforced concrete beams subjected to shear using the modified compression field theory. ACI Struct J 1988;85(4):258–68.
[22] Bentz EC, Vecchio FJ, Collins MP. Simplified modified compression field theory for calculating shear strength of reinforced concrete elements. ACI Struct J 2006;103(4):614–24.
[23] Pang XB, Hsu TTC. Behavior of reinforced concrete membrane elements in shear. ACI Struct J 1995;92(6):665–79.
[24] Hsu TTC. Toward a unified nomenclature for reinforced-concrete theory. J Struct Eng 1996;122(3):275–83.
[25] Pang XB, Hsu TTC. Fixed angle softened truss model for reinforced concrete. ACI Struct J 1996;93(2):197–207.
[26] Hsu TTC, Zhang LX. Nonlinear analysis of membrane elements by fixed-angle softened-truss model. ACI Struct J 1997;94(5):483–92.
[27] Schlaich J, Shafer K, Jennewein M. Toward a consistent design of structural concrete. PCI Journal 1987;32(3):74–150.
[28] Hwang SJ, Lee HJ. Strength prediction for discontinuity regions by softened strut-and-tie model. J Struct Eng 2002;128(12):1519–26.
[29] Committee ACI. 445. Recent approaches to shear design of structural concrete. J Struct Eng 1998;124(7):1375–417.
[30] Li VC, Mishra DK, Naaman AE, Wight JK, LaFave JM, Wu H-C, et al. On the shear behavior of engineered cementitious composites. Adv Cem Based Mater 1994;1(3):142–9.
[31] van Zijl GPAG. Improved mechanical performance: Shear behaviour of strain-hardening cement-based composites (SHCC). Cem Concr Res 2007;37(8):1241–7.
[32] Xu SL, Hou LJ, Zhang XF. Flexural and shear behaviors of reinforced ultrahigh toughness cementitious composite beams without web reinforcement under concentrated load. Engineering Structure 2012;39:176–86.
[33] Xu S, Hou L-J, Zhang X-F. Shear behavior of reinforced ultrahigh toughness cementitious composite beams without transverse reinforcement. Journal of Material in Civil Engineering 2012;24(10):1283–94.
[34] Hou L-J, Xu S, Zhang X-F, Chen Da. Shear behaviors of reinforced ultrahigh toughness cementitious composite slender beams with stirrups. Journal of Material in Civil Engineering 2014;26(3):466–75.
[35] Paegle I, Fischer G. Phenomenological interpretation of the shear behavior of reinforced engineered cementitious composite beams. Cem Concr Compos 2016;73:213–25.
[36] Kanda T, Lin Z, Li VC. Application of pseudo strain-hardening cementitious composites to shear resistant structural elements. 3rd International Conference on Fracture Mechanics of Concrete and Concrete Structures. Gifu, Japan: International Association of Fracture Mechanics for Concrete and Concrete Structures; 1998. p. 1477-90.
[37] Shimizu K, Kanakubo T, Kanda T, Nagai S. Shear behavior of steel reinforced PVA-ECC beams. 13th World Conference on Earthquake Engineering. Vancouver, B.C., Canada: World Conference on Earthquake Engineering; 2004.

[38] Kanakubo T, Shimizu K, Kanda T, Nagai S. In: Evaluation of bending and shear capacities of HPFRCC members toward the structural application. Sapporo, Japan: Hokkaido University; 2007. p. 1–10.
[39] Kanakubo T, Shimizu K, Nagai S, Kanda T. Shear transmission on crack surface of ECC. In: 7th International Conference on Fracture Mechanics of Concrete and Concrete Structures. Jeju, Republic of Korea: International Association of Fracture Mechanics for Concrete and Concrete Structures; 2010. p. 1623–30.
[40] ACI (American Concrete Institute). Building code requirements for structural concrete and commentary. ACI 318-19, Farmington Hills, MI; 2019.
[41] JSCE (Japan Society of Civil Engineers). Standard specification for concrete structures. JSCE-02, Tokyo; 2002.
[42] MOHURD (Ministry of Housing and Urban-Rural Development of the People's Republic of China). Code for design of concrete structures. GB 50010-10, Beijing; 2010.
[43] CSA (Canadian Standards Association). Design of Concrete Structures. CSA A23.3-14, Mississauga, ON, Canada; 2014.
[44] JSCE (Japan Society of Civil Engineers). Recommendations for design and construction of high performance fiber reinforced cement composites with multiple fine cracks (HPFRCC). 2008.
[45] Lee JY, Kin UY. Effect of longitudinal tensile reinforcement ratio and shear span-depth ratio on minimum shear reinforcement in beams. ACI Struct J 2008;105(2):134–44.
[46] Lee JY, Lee DH, Lee JE, Choi SH. Shear behavior and diagonal crack width for reinforced concrete beams with high-strength shear reinforcement. ACI Struct J 2015;112(3):323–33.
[47] Arezoumandi M, Volz JS, Ortega CA, Myers JJ. Shear behavior of high-volume fly ash concrete versus conventional concrete: experimental study. J Struct Eng 2014;141(3):B4014006.
[48] Laskar A, Hsu TTC, Mo YL. Shear strengths of prestressed concrete beams part 1: experiments and shear design equations. ACI Struct J 2010;107(3):330–9.
[49] Li W, Leung CKY. Shear span–depth ratio effect on behavior of RC beam shear strengthened with full-wrapping FRP strip. J Compos Constr 2015;20(3):04015067.
[50] Munikrishna A, Hosny A, Rizkalla S, Zia P. Behavior of concrete beams reinforced with ASTM A1035 grade 100 stirrups under shear. ACI Struct J 2011;108(1):34–41.
[51] Poldon JJ, Hoult NA, Bentz EC. Distributed sensing in large reinforced concrete shear test. ACI Struct J 2019;116(5):235–45.
[52] Poldon JJ, Hoult NA, Bentz EC. Understanding Reinforcement Behavior Using Distributed Measurements of Shear Tests. ACI Struct J 2021;118(3):255–66.
[53] Wu Y-F, Hu B. Shear Strength Components in Reinforced Concrete Members. J Struct Eng 2017;143(9):04017092.
[54] Hu B, Wu YF. Quantification of shear cracking in reinforced concrete beams. Eng Struct 2017;147:666–78.
[55] Hu B, Wu YF. Effect of shear span-to-depth ratio on shear strength components of RC beams. Eng Struct 2018;2018(168):770–83.
[56] Zhang ZG, Yuvaraj A, Di J, Qian SZ. Matrix design of light weight, high strength, high ductility ECC. Constr Build Mater 2019;210:188–97.
[57] Shao XX, Dai XJ, He XY. Noise robustness and parallel computation of the inverse compositional Gauss-Newton algorithm in digital image correlation. Opt Lasers Eng 2015;71:9–19.
[58] Shao XX, Dai YT, He XY, Wang HT, Wu G. Real-time digital image correlation for quasi-static test in civil engineering. Acta Optica Sinica 2015;35(10):1012003.
[59] Xu X, Ren X, Zhong F, Quan C, He X. Optimization of speckle pattern based on integer programming method. Opt Lasers Eng 2020;133:106100.
[60] Xu XY, Chen ZN, Huang Z, Tu YM, Wu G, He XY. Fabrication and application of digital speckle pattern in full-field measurement of deformed large concrete beams. Journal of Southeast University 2018;48(5):896–902.
[61] MIIT (Ministry of Industry and Information Technology of the People's Republic of China). Standard test method for the mechanical properties of ductile fiber reinforced cementitious composite. Building Industry Press, Beijing; 2018.
[62] Collins MP, Bentz EC, Sherwood EG. Where is shear reinforcement required? Review of research results and design procedures. ACI Struct J 2008;105(5):590–600.
[63] Park R, Paulay T, editors. Reinforced Concrete Structures. Wiley; 1975.
[64] Bandelt MJ, Billington SL. Bond behavior of steel reinforcement in high-performance fiber-reinforced cementitious composite flexural members. Mater Struct 2016;49(1–2):71–86.
[65] Dong LT, Pan JL, Yuan F, Leung CKY. Flexural behaviors of steel reinforced ECC/concrete composite beams. Journal of Southeast University (English Edition) 2012;28(2):195–202.